Politecnico di Torino

Politecnico di Torino

INGEGNERIA ENERGETICA E NUCLEARE

Sustainable Nuclear Energy

A.a. 2024/2025

Graduation Session

Optimising the few-group energy structure for the full-core simulation of Lead-cooled Fast Reactors

Supervisor:

Nicolò Abrate

Co-supervisor:

Alex Aimetta

Christian Vita

Sandra Dulla

Candidate:

Angela Costantino

Abstract

The objective this thesis is the application of genetic algorithm techniques to optimize the few-group energy grid for the multiphysics simulation of Lead-cooled Fast Reactors (LFR). The identification of a proper energy group structure to collapse the group constants to be used in full-core simulations is a crucial step: such energy structure has to be knowledgeably chosen as it may strongly affect the accuracy and efficiency of the multigroup calculation results. The energy grid structure to be used must be selected with the intention of preserving the physics of the problem, which is at the basis of accurate results, and to minimize as much as possible the computational effort involved in the simulation. This is true in general, but the problem complexity increases as we move towards fast spectrum fission reactions. In this framework, optimization techniques play a key role, as they are applied to a wide range of engineering fields, and the nuclear reactor physics is one of them. Starting from a set of feasible solutions, optimization techniques aim at identifying the nearly-optimal solutions by using proper objective functions, which are usually maximized or minimized, according to their definition. Evolutionary algorithms, and in particular Generic Algorithms (GAs), have revealed themselves to be powerful tools in solving high-dimensional, non-linear optimization problems. Inspired by the working principle of Darwinian selection and evolution, in recent years, GAs have been already tested in specific field of nuclear engineering: for example, they have been applied to optimize the energy grid structure for Molten Salt Reactors (MSR), providing encouraging results. Based on this outcome, it is interesting to evaluate and explore the performances and the possibilities related to the use of such techniques for the identification of the optimal energy group boundaries, focusing the attention on its application to the new Advanced Lead Fast Reactor European Demonstrator (ALFRED) benchmark, proposed by the Nuclear Energy Agency (NEA). To perform this study, the use of the multigroup diffusion module of the Fast REactor NEutronics/Thermal-hydrauliCs (FRENETIC) multiphysics code is adopted. Developed during the last decade at Politecnico di Torino, the code aims at simulating coupled neutronic/thermal-hydraulic transients in liquid-metal-cooled fast reactors with hexagonal subassemblies, providing

an approximated yet still reliable description of the physical behaviour of such technologies. Specifically, the code is used to evaluate the accuracy of few-group structures proposed by the GA, comparing them with a reference solution, provided by the Serpent2 Monte Carlo neutron transport code (which supplied quantities such as the effective multiplication factor, the radial and axial power distributions, etc.). The code is also exploited to retrieve the fine-grid nuclear data that need to be fed to neutronic module of the FRENETIC code as input parameters (e.g. macroscopic reaction cross sections, diffusion coefficient, etc.). To perform the comparison among the solutions, a set of physics-driven fitness functions (FFs) have been defined. Such FFs are related to the effective multiplication factor, to the power density, the neutron flux and the kinetic parameters, and turned out to be a suitable combination. The physical justification of the optimal solutions evaluated by the GA is confirmed through the evaluation of some significant figures of merit.

Table of Contents

Chapter 1

Introduction

1.1 Introduction

The objective of this thesis work is to apply the genetic algorithm technique to optimize the few-group energy structure for the multiphysics simulation of lead-cooled fast reactors.
The identification of a proper energy group structure to collapse the group constants for full-core simulations is a crucial step, as it strongly affects the reliability of the multigroup calculation results. For sure, the energy grid structure to be used must be selected with the intention of preserving the physical features of the problem, which helps to obtain accurate results, and of minimizing as much as possible the computational effort involved to retrieve the simulation outputs. This is true in general, but the problem complexity increases as we move towards fast spectrum fission reactions. In this framework, Genetic Algorithms play a key role.
In recent years, GAs have been applied to optimize the energy grid structure for molten salt reactors, providing encouraging results. Based on this, it is interesting to evaluate and explore the performances and the possibilities related to the use of such technique, focusing the attention on its application to the new Advanced Lead Fast Reactor European Demonstrator (ALFRED) benchmark.
To perform this study, the multigroup diffusion module of the Fast REactor NEutronics/Thermal-hydrauliCs (FRENETIC) [1] multiphysics code, developed during the last decade at Politecnico di Torino, will be employed to test the energy

group structures proposed by the GA. In addition, also the Serpent 2 [2] Monte Carlo code is exploited to retrieve the fine-grid nuclear data that need to be fed to FRENETIC as input parameters (e.g. macroscopic reaction cross sections, diffusion coefficient, etc.) but also to estimate some quantities of interest to carry out comparisons between the simulation results and assess their accuracy (e.g. effective multiplication factor, radial and axial power distributions, etc.).

To begin with, a brief overview of the neutron transport theory, the diffusion theory and the multigroup approach is presented in this chapter, with particular attention paid to the energy collapsing procedures.

1.1.1 Standard definitions

Given that the Neutron Transport Equation, the Diffusion Equation and the Multigroup Neutron Theory will be discussed in the upcoming sections, it is helpful to first review some essential definitions [3].
Let's indicate with t the time, with $\vec{r} = (x, y, z)$ the position, with E the energy, with $\vec{v}$ the velocity and with $\vec{\Omega} = \frac{\vec{v}}{|\vec{v}|}$ the direction. The direction in Cartesian coordinates is defined as follows:

$$\begin{cases} \vec{\Omega} = \Omega_x \vec{i} + \Omega_y \vec{j} + \Omega_z \vec{k} \\ \Omega_x^2 + \Omega_y^2 + \Omega_z^2 = 1 \end{cases} \tag{1.1}$$

However, since a spherical reference system is often preferred,

$$\begin{cases} \Omega_x = sin(\theta)cos(\phi) = \sqrt{1-\mu^2}cos(\phi), \\ \Omega_y = sin(\theta)sin(\phi) = \sqrt{1-\mu^2}sin(\phi), \\ \Omega_x = cos(\phi) = \mu, \end{cases} \tag{1.2}$$

we obtain:

$$\vec{\Omega} = \sqrt{1-\mu^2}cos(\phi)\vec{i} + \sqrt{1-mu^2}sin(\phi)\vec{j} + \mu\vec{k}. \tag{1.3}$$

The set of variables that have been introduced (position, energy, direction, time) define the so-called *phase space*, which represents a multidimensional space containing

all possible neutrons characterized by the combination of the dependent variables $(\vec{r}, E, \vec{\Omega}, t)$ of our interest. Instead, $n(\vec{r}, E, \vec{\Omega}, t)$ defines the neutron density function in the phase space, i.e .the number of neutrons per unit volume, energy, flying direction and time. By multiplying the neutron density for a an infinitesimal volume in the phase space $(d\vec{r}dEd\vec{\Omega})$

$$n(\vec{r}, E, \vec{\Omega}, t)d\vec{r}dEd\vec{\Omega} \tag{1.4}$$

we obtain the exact number of neutrons contained inside the geometrical volume $d\vec{r}$, having an energy in the range of $(E, E+dE)$ and characterized by a flying direction defined by the solid angle $d\vec{\Omega}$.
While traveling through matter, neutrons interact with its constituent atoms, potentially undergoing physical processes such as capture, fission, or scattering. Each kind of interaction is characterized by a certain probability of occurrence and this probability is indicated with the *macroscopic cross section* (Σ_x), where the subscript x represent a certain type of interaction. The macroscopic cross section represents the probability per unit path length that a specific event occurs. It is expressed in $\text{cm}^{-1}$and it is defined as:

$$\frac{NAs\sigma_x}{As} = N\sigma_x = \Sigma_x \tag{1.5}$$

Imagining a certain layer of area A (cm^2), thickness s (cm) and density of particles N (nuclei/cm^3), subjected to a neutron flux. Equation 1.5 defines the macroscopic cross section for that specific event *'x'* as the ratio between the total number of particles involved by the collision and the total volume of the medium. The first term can be obtained by multiplying the total number of medium particles by the area of particles involved in the collision. This quantity is a fundamental concept in nuclear physics, and it is called *microscopic cross section*. It is denoted by σ and defines the effective area that a target nucleus presents to an incoming particle for a given type of interaction, hence, it is evaluated in cm^2 (or b, 1 barn=10^{-24} cm^2) and quantifies the probability of occurrence for a specific interaction (e.g. fission, scattering, capture) between the incident particle and the target nucleus.

Now imagining a control volume close enough to an oriented area, so that the neutrons contained in dr can cross the infinitesimal area itself. The net flow of

neutrons is described by the *neutron current density vector* ($\vec{J}$). Hence, the net current evaluated through the whole closed surface can be expressed as:

$$\vec{J} = (\vec{r}, E, t) = \oint d\Omega \phi(\vec{r}, E, \vec{\Omega}, t)\vec{\Omega} \tag{1.6}$$

1.1.2 Neutron Transport Equation

The following neutron transport equation is wrote down considering an infinitesimal region of the phase space:

$$\begin{aligned}
&[n(\vec{r}, E, \vec{\Omega}, t + dt) - n(\vec{r}, E, \vec{\Omega}, t)]d\vec{r}dEd\Omega dt = \\
&= -\nabla \cdot \vec{\Omega}\Phi(\vec{r}, E, \Omega, t)d\vec{r}dEd\Omega dt + \\
&- \Sigma_t(\vec{r}, E)\Phi(\vec{r}, E, \Omega, t)d\vec{r}dEd\Omega dt + \\
&+ \oint d\Omega' \int_{-\infty}^{+\infty} dE' \Sigma_s(\vec{r}, E')\Phi(\vec{r}, E', \vec{\Omega}, t) f_s(\vec{r}, E' \rightarrow E, \vec{\Omega}' \cdot \vec{\Omega}) + \\
&+ S(\vec{r}, E, \vec{\Omega}, t)d\vec{r}dEd\Omega dt
\end{aligned} \tag{1.7}$$

The first term on the right-hand side of the equation takes into account the simple *streaming in space* of the neutrons moving through the medium, representing their net movement into or out of the infinitesimal control volume defined within the phase space under consideration. In the following, the second and third terms on the right-hand side, taken together, represent the *collision term* of the neutron transport equation. The former acts as a removal term: it models the neutrons within the phase space of interest that, after undergoing collisions, exit that phase space. Each type of collision is taken into account - this justifies the use of the total macroscopic cross section (Σ_t) - since every collision alters at least one of the variables defining the phase space, thereby making the neutron under investigation no longer relevant. The latter represents instead a source term for the phase space, as it takes into account all the neutrons, belonging to a phase space different from the one under investigation (to be more precise, the neutrons characterized by a different energy and/or a different angular direction), that become relevant right after a scattering collision. The term f_s requires particular attention, as it is strictly related to the probability that the neutron involved in the scattering interaction is emitted in the observed phase space right after the collision. In fact, the term f_s

is a *probability density function* and depends on the energy and angular direction owned by the neutron before (E', $\vec{\Omega}'$) and after ($E, \vec{\Omega}$) the collision. If the neutrons are moving through an isotropic medium, the probability does not depend on the incoming direction of the neutron but only on the angle between the two directions.

$$f_s(\vec{r}, E' \to E, \vec{\Omega}' \to \vec{\Omega}) \Rrightarrow f_s(\vec{r}, E' \to E, \vec{\Omega}' \cdot \vec{\Omega}) \tag{1.8}$$

To sum up, the terms appearing in the equation above have the following meanings, respectively:

[neutrons at time (t+dt)]-[neutrons at time (t)]=
= [neutrons moving in]-[neutrons moving out]+
-[collided neutrons]+[neutrons scattered in from outside]+
+[source]

Dividing Equation 1.7 by both the differential phase space ($d\vec{r}dEd\Omega$) and the infinitesimal time step (dt), and then deriving the equation in time, the infinitesimal increment in time of the neutron density is made explicit. Equation 1.7 now appears as:

$$\begin{aligned}\frac{\partial n(\vec{r}, E, \vec{\Omega}, t)}{\partial t} &= -\nabla \cdot \vec{\Omega}\Phi(\vec{r}, E, \vec{\Omega}, t) - \Sigma_t(\vec{r}, E, \vec{\Omega}, t)\Phi(\vec{r}, E, \vec{\Omega}, t) + \\ &+ \oint d\Omega' \int_{-\infty}^{+\infty} dE' \Sigma_s(\vec{r}, E')\Phi(\vec{r}, E', \vec{\Omega}', t) f_s(\vec{r}, E \to E', \vec{\Omega}' \cdot \vec{\Omega}) + \\ &+ S(\vec{r}, E, \vec{\Omega}, t)\end{aligned} \tag{1.9}$$

At this point, we can notice that there are two unknown variables, the neutron density, $n(\vec{r}, E, \vec{\Omega}, t)$, and the angular flux, $\Phi(\vec{r}, E, \vec{\Omega}, t)$, which are two quantities strictly related according to the following expression:

$$n(\vec{r}, E, \vec{\Omega}, t) = \frac{1}{\mathrm{v}}\Phi(\vec{r}, E, \vec{\Omega}, t) \tag{1.10}$$

Exploiting such relation allows us to retrieve the same unknown variable in both

sides of the equation:

$$\frac{1}{\mathtt{v}}\frac{\partial\Phi(\vec{r},E,\vec{\Omega},t)}{dt} = -\nabla\cdot\vec{\Omega}\Phi(\vec{r},E,\vec{\Omega},t) - \Sigma_t(\vec{r},E,\vec{\Omega},t)\Phi(\vec{r},E,\vec{\Omega},t)+ \quad (1.11)$$
$$+ \oint d\Omega' \int_{-\infty}^{+\infty} dE'\Sigma_s(\vec{r},E')\Phi(\vec{r},E',\vec{\Omega}',t)f_s(\vec{r},E\to E',\vec{\Omega}'\cdot\vec{\Omega})+$$
$$+ S(\vec{r},E,\vec{\Omega},t)$$

By looking at Equation 1.12, it can be observed that the only source term that allows neutrons to be added to the phase space following a collision is the scattering term. Hence, the equation is reformulated, now including the contribution given by the fission term:

$$\frac{1}{\mathtt{v}}\frac{\partial\Phi(\vec{r},E,\vec{\Omega},t)}{dt} = -\nabla\cdot\vec{\Omega}\Phi(\vec{r},E,\vec{\Omega},t) - \Sigma_t(\vec{r},E,\vec{\Omega},t)\Phi(\vec{r},E,\vec{\Omega},t)+ \quad (1.12)$$
$$+ \oint d\Omega' \int_{-\infty}^{+\infty} dE'\Sigma_s(\vec{r},E')\Phi(\vec{r},E',\vec{\Omega}',t)f_s(\vec{r},E\to E',\vec{\Omega}'\cdot\vec{\Omega})+$$
$$+ \oint d\Omega' \int dE'\nu(\vec{r},E')\Sigma_f(\vec{r},E')\Phi(\vec{r},E',\vec{\Omega},t)\frac{\chi(\vec{r},E)}{4\pi}$$
$$+ S(\vec{r},E,\vec{\Omega},t)$$

The only difference in modeling the fission interaction with respect to the scattering ones stands in the number of neutrons emitted after the interaction. In fact, the term $\nu(\vec{r},E')$ represents the number of neutrons emitted right after a fission interaction involving a neutron with energy E'. Despite being formally defined in a different way, the *fission spectrum* term $\chi(\vec{r},E)$ has the same meaning of the probability density function in scattering collisions: it represents the probability for the neutron generated by fission to be emitted in the energy range of interest. The fission spectrum does not contain any information about the flying direction of the emitted neutrons, as fission can be considered isotropic, hence, the probability for a neutron to be reissued in a certain direction is the same for all the directions (i.e $\frac{1}{4\pi}$). Because of the nature of the neutron transport equation, some spatial and time boundary conditions are needed. Some approximation can be made, for example: the domain can be considered as a non-re-entering and simply-connected one. This approximation allows to assess that neutrons that exits the domain are

lost. In addition, since the system is surrounded by air, that can be considered as nearly vacuum environment, no neutrons can enter the domain from the outside.

$$\begin{cases} \phi(\vec{r}, E, \vec{\Omega}, t = 0 = \phi_0(\vec{r}, E, \vec{\Omega}) \\ \phi(\vec{r}, E, \vec{\Omega}_{in,t}) = 0 \end{cases} \tag{1.13}$$

The steady state transport equation with a null neutron source is an homogeneous problem which assures a null solution. In order to assure the same equation allows a non-trivial solution, the introduction of the k eigenvalue is needed, to which is associated an eigenfunction solution.

$$\hat{L}\Phi(\vec{r}, E, \vec{\Omega}) = \frac{1}{k}\hat{F}\Phi(\vec{r}, E, \vec{\Omega}) \tag{1.14}$$

The equation can be solved through an iterative process called *power method*, which is needed due to the nature of the operators appearing in equation 1.14, which is the operatorial expression of the steady state NTE with negligible source. The power method allows to solve for the eigenvalue and the neutron flux, and within the k value some important features of the systems are hold:

- when $k = 1$ the system is called critical, this means that the system is self-sustaining, meaning that the fission reactions compensate the neutron losses;
- when $k > 1$ the system is called supercritical, meaning that neutrons produced by fission are much more that the ones that are lost;
- when $k < 1$ the system is called subcritical, fission cannot withstand the leakages and an external source is needed.

The transport phenomena at the basis of the NTE are relatively easy to derive but, on the other hand, the transport equation may not be so easy to be solved. An alternative to the transport theory that yet provide a good approximation of the exact transport solution is given by the *diffusion theory*, which comes out from a simplification of the NTE under certain conditions. This theory will be briefly described in the following section, as it is at the basis of the multiphysics FRENETIC code employed in this study.

1.1.3 Diffusion Equation

Let's start again from the neutron balance already appearing in the previous section, but with a slight different form:

[neutrons at time (t+dt)]-[neutrons at time (t)]=
= [neutrons moving in]-[neutrons moving out]+
-[neutrons absorbed in (t, t+dt)]+[source]

which can be re-written as:

$$\frac{\partial n(\vec{r}, t+dt)}{\partial t} = -\nabla \cdot \vec{J}(\vec{r}, t) - \Sigma_a(\vec{r})\phi(\vec{r}, t) + S(\vec{r}, t) \tag{1.15}$$

At the basis of the diffusion theory there is the intuition that the relationship between the neutron flux and the neutron current density can be described through the Fick's law, which states that the neutron current density vector is proportional to the negative gradient of the flux according to the diffusion coefficient:

$$\vec{J}(\vec{r}, t) = -D(\vec{r})\nabla\Phi(\vec{r}, t) \tag{1.16}$$

$$D = \frac{\Sigma_s}{3\Sigma_t^2} \tag{1.17}$$

This closure relationship can be exploited and included in Eq. 1.18, as long as some conditions are met:

- the scattering is isotropic and predominant over absorption;
- quasi isotropy of the neutron flux.

In this way, equation 1.18 becomes:

$$\frac{1}{\mathtt{v}}\frac{\partial\phi(\vec{r}, t)}{\partial t} = +\nabla \cdot D(\vec{r})\nabla\phi(\vec{r}, t) - \Sigma_a(\vec{r})\phi(\vec{r}, t) + S(\vec{r}, t) \tag{1.18}$$

The scattering term does not appear in this equation, as the information regarding this kind of interaction is embedded in the diffusion coefficient, as it can be considered the cause of neutrons motion described by Fick's law itself. In the case

of steady state, the equation simply becomes:

$$\nabla \cdot D(\vec{r})\nabla\phi(\vec{r},t) - \Sigma_a(\vec{r})\phi(\vec{r},t) + S(\vec{r},t) = 0 \tag{1.19}$$

As the diffusion equation is a partial differential equation, it assures an infinite number of solutions, hence, physical boundary conditions are needed in order to identify the one function that can be physically accepted. To begin with, the boundary condition at the surface will be briefly described. It is based on the fact that the neutron flux does not reach the null value at the system physical boundary, but is surely decreases, since outside the reactor there is an essentially vacuous media. Hence, the neutron flux becomes null at the so called *extrapolated distance (d)*, which assumes different expression according to the geometry of the system. In the case of a planar free surface, the extrapolation length assumes the expression $d = 0.71\lambda_{tr}$, valid in the case of a non-re-entrant reactor surface (where λ_{tr} is the transport mean free path of the medium), while in the case of cylindrical free surface, it is dependent on the curvature radius of the surface itself.

$$\frac{1}{\phi}\frac{d\phi}{dn} = -\frac{1}{d} \tag{1.20}$$

In the case of a real non uniform reactor, it is important to identify the behavior of the neutron flux and the neutron current density at the interfaces between the materials. The former is indeed continuous at the interface between two different media, while, for what concerns the latter, the following expression must be observed:

$$(J_A)_n = (J_B)_n \tag{1.21}$$

This expression states that the normal component of the neutron current density computed at the interface of A material region is equal to the net number of neutrons per unit area leaving/entering that region, which is equal to the number of neutrons entering/leaving the adjacent region. In the case of a time-dependent problem, the shape of the neutron flux must be known apriori.

$$\phi(\vec{r}, t = 0) = \phi_0(\vec{r}) \tag{1.22}$$

For both the Diffusion Theory and the Transport Theory a multigroup approach can be applied.

1.1.4 Multigroup Theory

The multigroup theory is a fundamental tool in the framework of nuclear reactor physics modeling, as it strongly simplifies the problem associated with energy dependency of neutrons. Neutrons propagating through the medium are characterized by a broad energy spectrum: those originating from fission reactions are emitted with energies in the range of MeV (commonly referred to as *fast neutrons*). As they travel through the medium, they are slowed down due to successive scattering interactions that may eventually bring the neutrons to reach energies contents in the range of eV (classified as *slow neutrons*, or *thermal neutrons*). As it can be expected, handling the continuous-energy spectrum that characterizes the neutrons is computationally demanding. To cope with this issue, the multigroup theory splits the broad energy spectrum into a finite number of smaller intervals, called *groups*. Within each energy group, the cross sections are represented by average values, hence, the energy dependence is approximated as a discrete set of group-wise averages. This implies that, starting from the NTE, by using the multigroup theory we end up with a *set* of equation, one for each group, which are fully coupled.
The energy groups are numbered in descending order, starting from the most energetic group (identified as *g=1*), while the energy group boundaries are labeled with E_g.
The steps required to simplify the scattering term will not be addressed in this section, as they are not relevant in the present discussion. Hence, the *steady-state multigroup transport equation* appears as:

$$\vec{\Omega}\cdot\nabla\phi_g(\vec{r},\vec{\Omega})+\Sigma_{t,g}(\vec{r},\vec{\Omega})\phi_g(\vec{r},\vec{\Omega})=\sum_{n=0}^{\infty}\sum_{\beta=-n}^{\beta=+n}\sum_{g'}^{G}\Sigma_{n,g'\to g}(\vec{r})\phi_{n,g'}^{\beta}(\vec{r})Y_n^{\beta}(\vec{\Omega})+ \quad (1.23)$$

$$+\frac{\chi_g}{4\pi}\sum_{g'}^{G}\nu_{g'}(\vec{r})\Sigma_{f,g'}(\vec{r})\Phi_{g'}(\vec{r})+S_g(\vec{r},\vec{\Omega})$$

The macroscopic cross sections are obtained by an *averaging* process, often referred to as *collapsing*, which consists in averaging the cross section over a certain energy

interval by preserving the number of collisions in the group. For a generic cross-section ($\Sigma_x(\vec{r}, E, \vec{\Omega})$):

$$\Sigma_{x,g} = \frac{\oint \int_{E_{g-1}}^{E_g} \Sigma_x(\vec{r}, E)\phi(\vec{r}, \vec{\Omega}, E)dEd\Omega}{\oint \int_{E_{g-1}}^{E_g} \phi(\vec{r}, \vec{\Omega}, E)dEd\Omega} \tag{1.24}$$

The term $\Sigma_{n,g'\to g}(\vec{r})$ appearing in Equation 1.23 is called *energy transfer matrix* and it may serve as the *scattering matrix* when the latter includes all forms of scattering (elastic, inelastic, isotropic/anisotropic).

1.1.5 The adjoint flux

In this paragraph the adjoint flux and its interpretation are going to be introduced as it will be exploited within the GA, as a significant key quantity in the design of a reactor. As follows, the importance function is going to be expressed as

$$\psi(\vec{r}, E, \vec{\Omega}) \tag{1.25}$$

that is going to be intended as measure of how much *important* the neutron in a certain phase space is in the framework of undergo fission reactions. Because of the isotropic nature of the fission process, the importance quantity can be considered a conservative one. Considering a certain number of neutrons (N) moving towards a certain direction from a starting point r up to a nearby one $\vec{r}+ds\vec{\Omega}$: the importance of neutrons located in r needs, hence, to be equal to the sum of the importance of neutrons survived up to $\vec{r}+ds\vec{\Omega}$, the one of neutrons scattered along the way and the one of the neutrons that undergone fission in the phase space of interest. The overall balance can be hence defined as:

$$\begin{aligned} &N_0\psi(\vec{r}, E, \vec{\Omega}) = N_0(1 - \Sigma(\vec{r}, E)ds)\psi(\vec{r} + ds\vec{\Omega}, E, \vec{\Omega}) + \\ &+ N_0\Sigma_s(\vec{r}, E)ds \int dE' \oint d\Omega' f_s(\vec{r}, E \to E', \Omega \to \vec{\Omega}')\psi(\vec{r}, E, \vec{\Omega}) + \\ &+ N_0 ds \frac{1}{k} \int dE' \oint d\Omega' \nu(\vec{r}, E)\Sigma_f(\vec{r}, E)\frac{\chi(\vec{r}, E'}{4\pi}\psi(\vec{r}, E', \vec{\Omega}') \end{aligned} \tag{1.26}$$

By simplifying N_0 and ds and by taking the limit for $ds \to 0$, the expression appears as follows:

$$\begin{aligned} &-\vec{\Omega}\cdot\nabla\psi(\vec{r},E,\vec{\Omega})+\Sigma(\vec{r},E)\psi(\vec{r},E,\vec{\Omega})= \\ &\int dE'\oint d\Omega' f_s(\vec{r},E\to E',\Omega\to\vec{\Omega}'\psi(\vec{r},E,\vec{\Omega})+ \\ &+\frac{1}{k}\int dE'\oint d\Omega'\nu(\vec{r},E)\Sigma_f(\vec{r},E)\frac{\chi(\vec{r},E'}{4\pi}\psi(\vec{r},E',\vec{\Omega}') \end{aligned} \tag{1.27}$$

This equation, that already strongly recall the nature of the NTE, needs a boundary condition, which states that no neutrons can enter the system from the external world and, for the same reason, every neutron exiting the system is considered to be lost: the importance of those neutrons is null.

$$\psi(\vec{r_s},E,\vec{\Omega}_{out}) \tag{1.28}$$

As anticipated, this paragraph is not going to discuss the mathematical adjoint operators, but is still relevant to asses that their application is fundamental to highlight the relationship between the neutron flux and the importance function. Indeed, it can be demonstrated that the neutron flux is the adjoint function of the importance, and vice-versa [3].

$$\psi=\phi^+ \tag{1.29}$$

1.1.6 Feedback

In this section, the feedback mechanisms of nuclear power system are going to be briefly discussed, focusing on their effect on fast spectrum nuclear power reactors. Feedback effects play a crucial role in the reactor control as they strongly affect the reactivity of the system following some changes in the up-to-now stable reactor conditions. Feedback mechanisms can be classified into two main categories: *positive feedback* and *negative feedback*, as they can, respectively, either enhance the condition that caused them or lessen them. Hence, it is crucial to try to predict apriori how certain reactor condition modifications affect the reactivity. The main contributions associated to the feedback effects are due to the *Doppler broadening* of the resonance cross-section in fertile material, the fuel and coolant thermal

expansions due to the change in densities, the coolant temperature feedback and the hardening of the thermal spectrum. As follows, the fuel feedback mechanisms strictly related to temperature field is going to be considered.

Fuel temperature feedback

A potential increase of the fuel temperature has the well known consequential effect of changing the fuel density and absorption cross sections of neutrons at resonance energies. The former phenomena has usually a very small impact in reactors with ceramic fuel pellets, as they are characterized by generally small expansion coefficient, and it is to be considered a negative reactivity effect as neutron leakages increase. The latter phenomenon is usually referred to as the *Doppler effect*. It depends on the neutron absorption cross-sections, that tends to increase at the resonance peaks characteristic of fertile nuclides. By looking at figure 1.1, it can be noticed that at stable reactor conditions (*unbroadened*), only neutrons with an energy content very close to E_0 are likely to be absorbed. As the fuel temperature increases, the thermal motion of the fuel nuclei allows to get to a wider distribution of the neutron energies around the E_0 value, then broadening the distribution of the absorption cross sections of neutrons around E_0.

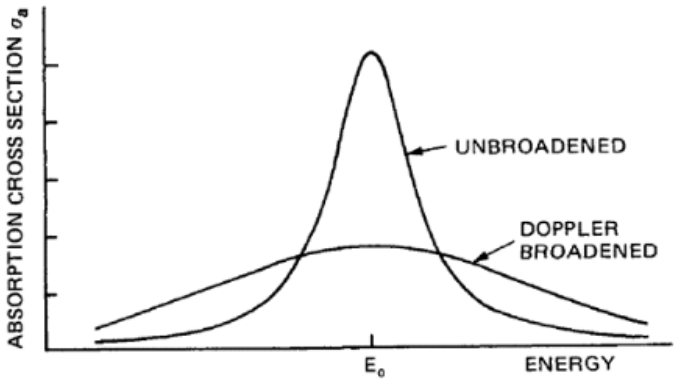

Figure 1.1: Effect of temperature on the effective shape of a resonance absorption cross-section [4]

.

Doppler effect can produce either a positive or negative feedback effect according to the fissile content of the fuel: if the fuel is primarily fissile, the absorption

at the resonance region occurs in the form of fission reactions, increasing the multiplication factor, while if the fuel fissile content is "low", the parasitic capture are predominant.

Chapter 2

Methodology

In this chapter an overview of the tools and technologies that has been employed throughout the development of this thesis project will be provided. This includes a detailed descriptions of the preliminary steps that has been taken before the application of the Genetic Algorithm. This setup phase has been crucial and essential to set up the working environment for the project. Hence, in the following sections particular attention will be given to the **Serpent2 Monte Carlo neutron transport code** and the multigroup diffusion module of the **Fast REactor NEutronics/Thermal-hydrauliCs (FRENETIC) multiphysics** one, while the Genetic Algorithm core tool will be deeply described in the following chapter.

2.1 System geometry description

As anticipated in the introduction section, this thesis works aims to apply the Genetic Algorithm to the Advanced Lead Fast Reactor European Demonstrator (ALFRED), which is one of the most promising designs of the new Generation-IV nuclear energy systems. ALFRED is a Lead-cooled Fast Reactor, which seems to encounter many of the needs and goals of Generation-IV reactors, such as sustainability, safety and reliability.
ALFRED is a 300 MWth pool-type fast reactor operating in the 400°C-520°C (respectively, core inlet temperature and average core outlet temperature) temperature window. The main characteristic of this system is the absence of the

moderator, which is instead replaced with liquid lead acting as a coolant, that, being a low-moderating medium, is characterized by a low neutron absorption cross section.
The inner core is composed of 253 hexagonal sub-assemblies arranged with a triangular pitch and are organized as follows:

- 56 inner fuel assemblies (IF);
- 78 outer fuel assemblies (OF);
- 12 control rods (CR);
- 4 safety rods (SR);
- 48 reflector assemblies (RAs)
- 54 shield assemblies (SAs);
- 1 test assembly (TA).

Reflector assemblies, shield assemblies and the test assembly are all modeled as fuel assemblies, with Yttria-Stabilized Zirconia (YSZ) pellets stacked in a column occupying what in the FA would have been the plenum region, the insulator region and the fuel one. The core is enclosed by the barrel component and surrounded by the downcomer. The former is made by low-carbon chromium-nickel stainless steel and serves as a support structure that houses the inner reactor core, while the latter, being the region in between the barrel and the reactor vessel, is filled with the coolant (that will be referred to as *external lead*). Both those components are still modeled as hexagonal sub-assemblies both in the Serpent2 model and in the FRENETIC one.

Lead-cooled Fast Reactors give strong support from the point of view of sustainability: the operation at a fast neutron spectrum gives the possibility to use recycled plutonium and depleted uranium in the form of Mixed Oxides (MOX) fuel. The uranium-plutonium mixed oxides have two different enrichment levels, one for the inner and one for the outer core regions. The isotopic composition of uranium and plutonium are listed in the following table (Table 2.1)

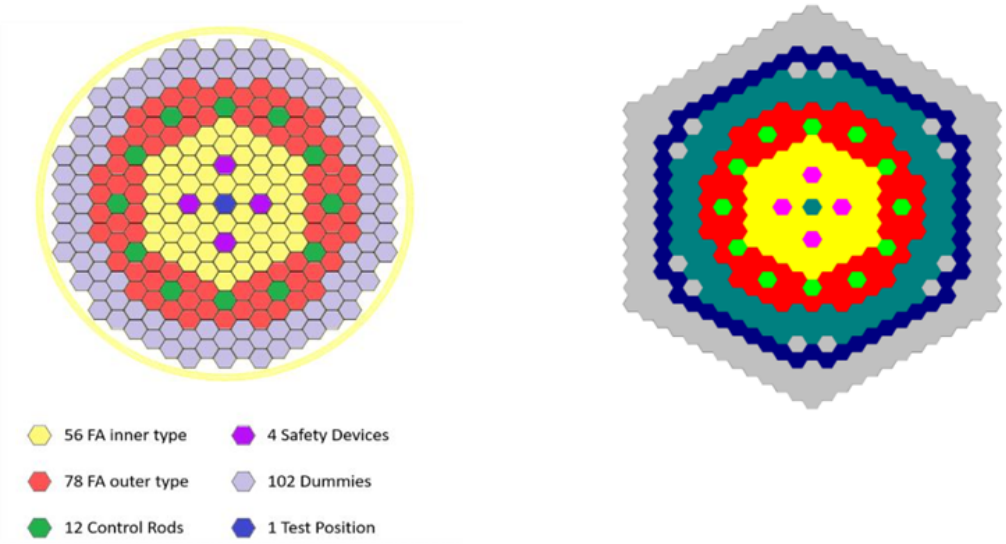

Figure 2.1: ALFRED core map and core model [5].

Parameter	Nominal Value	
Uranium vector:	Weight percent	Atom percent
U-234	0.00066%	0.00067%
U-235	0.20000%	0.20255%
U-238	99.79934%	99.79678%
Plutonium vector:	Weight percent	Atom percent
Pu-238	2.30168%	2.31733%
Pu-239	56.13464%	56.27911%
Pu-240	26.64604%	26.60315%
Pu-241	6.02465%	5.98992%
Pu-242	7.59299%	7.51798%
Am-241	1.30000%	1.29251%

Table 2.1: Uranium and Plutonium isotopic composition.

For what concerns the control rods, they are both used for reactor control and during the shutdown procedure. Hence, due to the dual function they serve, the neutron absorber employed, boron carbide (^{10}B), has been divided into two

separate sections, which differ in their enrichment levels and are listed in table 2.2. Reactor shutdown is managed not only by the control rods (CRs), but also by the safety rods (SRs), which are specifically designed to offer a redundant and diverse shutdown mechanism. Similarly to the control rods, the safety rods are inserted into the core from the bottom.

Parameter	Nominal value
Lowe absorber region	
^{10}B enrichment	90.0 at.%
density	2.2012 g/cm^3
length	45 cm
Upper absorber region	
^{10} B enrichment	42 at.%
density	2.2814 g/cm^3
length	40.5 cm

Table 2.2: ^{10}B data in control rods.

2.2 Serpent2 Monte Carlo code model set up

In this section, the Serpent2 model of the ALFRED conceptual core is going to be depicted. Serpent is a continuous-energy Monte Carlo Reactor Physics Burnup Calculation Code developed at VTT - Technical Research Centre of Finland. As suggested, it is based on the Monte Carlo statistical method, a computational technique very efficient in simulating complex problems characterized by random processes associated with a known probability density function representative of the event under investigation, throughout a repeated statistical sampling. In the framework of this thesis work, the latest version 2.2.1 published in March 2023 has been used. Among its several applications, in this work the Serpent2 code is going to be exploited because of its capability in calculating homogenized multi-group cross sections, kinetic parameters, scattering matrix and diffusion coefficient for the fine grid energy structure fed to the code, and in evaluating different neutronic

parameters such as the multiplication factor (k_{eff}), power and flux distributions.

In the following paragraphs, the ALFRED geometry modeling will be briefly described, along with the tools implemented in order to assess the temperature distribution effect on the geometry and the definition of the standard detector employed to calculate the flux and the power distributions. In addition, the *minicore* strategy exploited in this work with the intent of improving the statistics associated to the group constants will be described.

2.2.1 ALFRED conceptual core modeling

The construction of the representative geometric model of the ALFRED core using Serpent2 serves as the starting point of this thesis work. This process involves writing an input file composed of keywords known as 'cards', each of which defines a specific information about the geometric structure. A key piece of information to note is that Serpent uses a universe-based geometry model: this means that the geometry of the core needs to be built step by step with different separate levels, which are developed independently one to the other, and that according to their combination allow to build the resultant geometry. The independent levels, starting from the fuel pin up to the full core, are then nested one inside the other. The major process to build the reactor core is now briefly discussed. Starting from the inner level, the core geometry modeling begins with the definition of the pins. Pins are defined independently in their own universe with set of nested annular layers characterized by an homogeneous material. They do not correspond to an actual geometry object, but to a macro-structure needed to define the the assembly lattice. Indeed, the lattices are universes filled with other universes arranged with a regular structure. An example is specified as follows, which represent the fuel pins whose structure is given by the fuel pellets, surrounded by the cladding and the coolant and arranged with a triangular lattice within an hexagonal assembly, fig. 2.2. The three-dimensional feature of the reactor core model is instead given by the use of the *cell* card. Cells define a three-dimensional space throughout a set of positive and negative surface, which have been previously defined by the *surf* card. Each assembly is defined as a set of cells vertically stacked one upon the other. Each cell is filled with a universe, and the collection of universes filling these

```
pin pi      % inner fuel pin
helium     0.01
mox_in     0.455
helium     0.465
aim1       0.525
lead2

% -- inner fuel lattice
lat finn 2 0.0 0.0 15 15 1.36 %1.36
l1 l2 l2 l2 l2 l2 l2 l2 l2 l2 l2 l2 l2 l2 l2
 l2 l2 l2 l2 l2 l2 l2 pi pi pi pi pi pi pi l2
  l2 l2 l2 l2 l2 l2 pi pi pi pi pi pi pi pi l2
   l2 l2 l2 l2 l2 pi pi pi pi pi pi pi pi pi l2
    l2 l2 l2 l2 pi pi pi pi pi pi pi pi pi pi l2
     l2 l2 l2 pi pi pi pi pi pi pi pi pi pi pi l2
      l2 l2 pi pi pi pi pi pi pi pi pi pi pi pi l2
       l2 pi pi pi pi pi pi h2 pi pi pi pi pi pi l2
        l2 pi pi pi pi pi pi pi pi pi pi pi pi l2 l2
         l2 pi pi pi pi pi pi pi pi pi pi pi l2 l2 l2
          l2 pi pi pi pi pi pi pi pi pi pi l2 l2 l2 l2
           l2 pi pi pi pi pi pi pi pi pi l2 l2 l2 l2 l2
            l2 pi pi pi pi pi pi pi pi l2 l2 l2 l2 l2 l2
             l2 pi pi pi pi pi pi pi l2 l2 l2 l2 l2 l2 l2
              l2 l2 l2 l2 l2 l2 l2 l2 l2 l2 l2 l2 l2 l2 l2
```

Figure 2.2: Inner fuel pin and lattice definition

cells represents, in the framework of this work, the homogenized materials whose nuclear data have been evaluated and collapsed over a fine-group energy structure (tab. 2.5). Once every type of assembly has been defined according to the process just mentioned, they are re-arranged in the full-core hexagonal lattice.
The universes filling the cells have been defined with the criterion of trying to preserve as much as possible the material discretization of the rods along the axial dimension.
In this project, three different reactor core configurations have been identified and a Serpent2 3D model has been built for each of them:

- control rods fully withdrawn (*CRout*);
- control rods partially inserted (*CRin0*): in such a way that the active region of the control rods faces the fuel assembly one for a length of 28 cm;

- control rods fully inserted (*CRin55*): the fuel fully faces the absorber contained in the control rods.

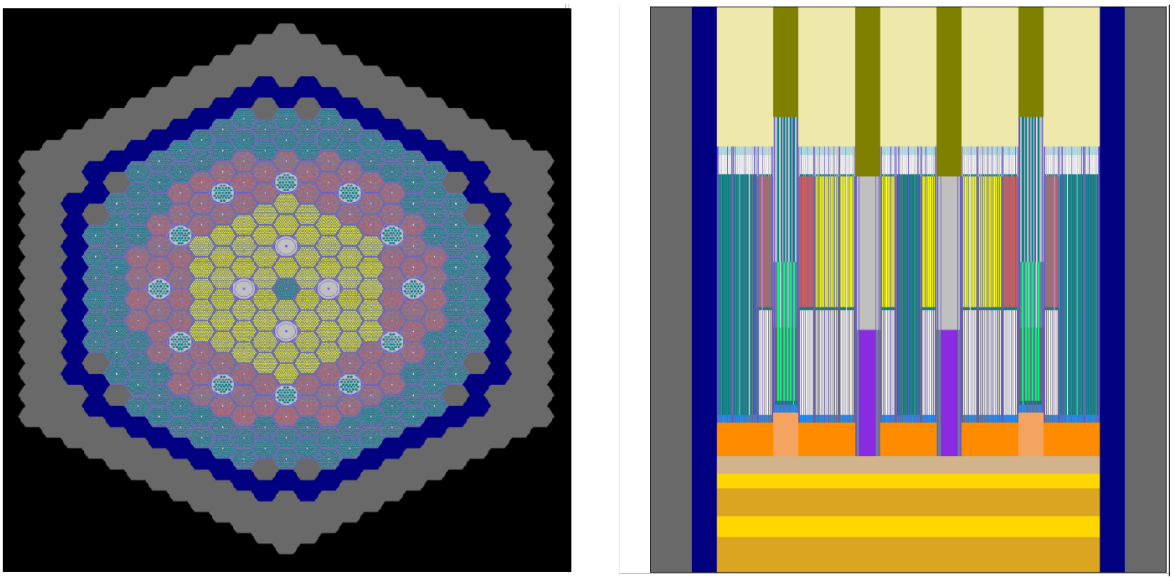

Figure 2.3: Radial view on ALFRED core (left) and axial view with CR partially inserted (right).

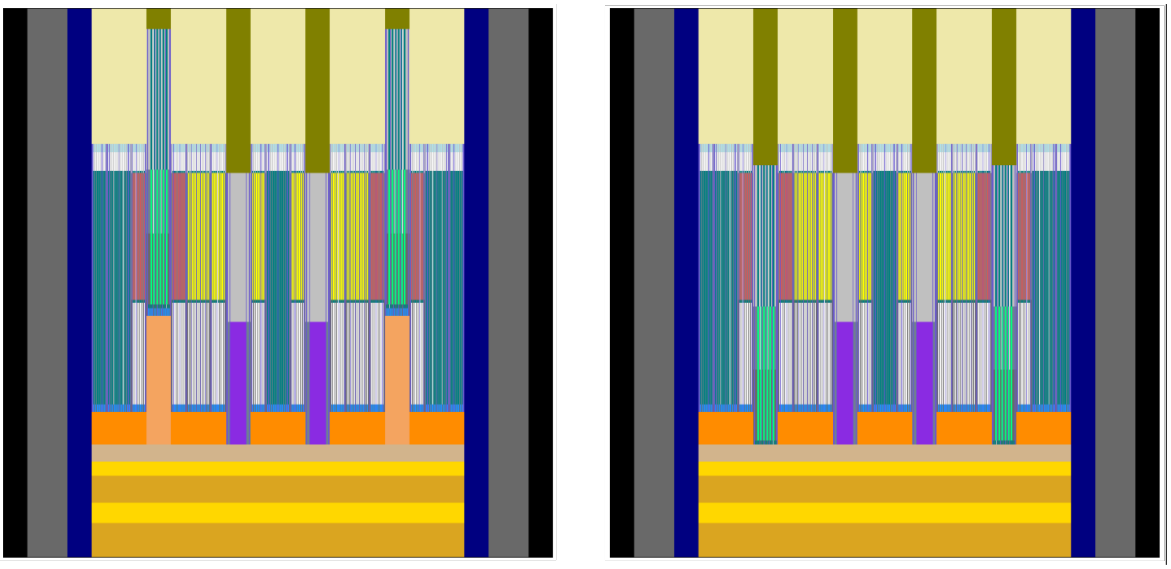

Figure 2.4: Axial view on ALFRED-NEA core with CR fully inserted (left) and CR withdrawn (right).

In order to retrieve the reference power and the neutron flux distributions within

the reactor core, detectors need to be defined within the Monte Carlo model. Detectors are the key tools needed to extract and elaborate results coming from the Serpent2 simulation, with the aim of measuring the meaningful quantity of interest. Their definition depends on the specific goals one want to achieve: in this project, the detectors have been defined as virtual volumes super-imposed to the whole previously defined geometry. To be more precise, they have been built afterwards the identification of a proper axial discretization in FRENETIC: indeed, detectors appears as a set of volumes that covers the whole axial extension of each assembly, following the discretization used within the diffusion code and taking into account the number of nodes for each axial bin (fig. 2.5). For what concerns the detectors used for power distribution evaluation, the use of the key words "dr -8 void" allows to actually evaluate the total *fission* energy deposition. Results, for both flux and power distributions, will be collected according to the energy grid structure defined within the model.

```
det flux0  n            dh 3 0 0 16.7 33 33 0     61    3 de EN37G
det flux1  n            dh 3 0 0 16.7 33 33 61    97.5  2 de EN37G
det flux2  n            dh 3 0 0 16.7 33 33 97.5  106.5 1 de EN37G
det flux3  n            dh 3 0 0 16.7 33 33 106.5 159.0 3 de EN37G
det flux4  n            dh 3 0 0 16.7 33 33 159.0 164.0 1 de EN37G
det flux5  n            dh 3 0 0 16.7 33 33 164.0 192.0 3 de EN37G
det flux6  n            dh 3 0 0 16.7 33 33 192.0 245.0 5 de EN37G
det flux7  n            dh 3 0 0 16.7 33 33 245.0 250.0 1 de EN37G
det flux8  n            dh 3 0 0 16.7 33 33 250.0 263.5 1 de EN37G
det flux9  n            dh 3 0 0 16.7 33 33 263.5 350   4 de EN37G

det powr0  n dr -8 void dh 3 0 0 16.7 33 33 0     61    3 de EN37G
det powr1  n dr -8 void dh 3 0 0 16.7 33 33 61    97.5  2 de EN37G
det powr2  n dr -8 void dh 3 0 0 16.7 33 33 97.5  106.5 1 de EN37G
det powr3  n dr -8 void dh 3 0 0 16.7 33 33 106.5 159.0 3 de EN37G
det powr4  n dr -8 void dh 3 0 0 16.7 33 33 159.0 164.0 1 de EN37G
det powr5  n dr -8 void dh 3 0 0 16.7 33 33 164   192.0 3 de EN37G
det powr6  n dr -8 void dh 3 0 0 16.7 33 33 192   245.0 5 de EN37G
det powr7  n dr -8 void dh 3 0 0 16.7 33 33 245   250.0 1 de EN37G
det powr8  n dr -8 void dh 3 0 0 16.7 33 33 250   263.5 1 de EN37G
det powr9  n dr -8 void dh 3 0 0 16.7 33 33 263.5 350   4 de EN37G
```

Figure 2.5: Detector definition in Serpent 2 input file.

At the beginning of this project, the reactor has been intended at isothermal

conditions, with all the materials' temperatures set equal to *673 K*. Since this projects also aims at introducing the cross-section feedback effect established by the temperature distribution, some adjustments to the original model of the reactors are needed. This means that the reactor core model procedure must be repeated taking into account the different temperatures between coolant and fuel to reconstruct the cross section database to be fed to the diffusion code: this is done for each core configuration and for each temperature set reported in table 2.3.

	T_c=**673 K**	T_c=**1073 K**	T_c=**1473 K**
T_f=**673 K**	x		
T_f=**1073 K**	x	x	
T_f=**1473 K**	x	x	x

Table 2.3: Temperature set to be implemented in Serpent 2 to reconstruct the cross section database and account for feedback effect.

Some modifications to the original Serpent2 input file have been introduced in order to obtain a reference power distribution for each temperature set. This is needed to knowledgeably analyze the outcomes coming from coupled neutronic/thermal-hydraulic simulations. Hence, the fuel active region have been further axially discretized into three regions, with the same axial extension. Moreover, the inner fuel have been radially discretized, being divided into two regions, as well has for the outer fuel, that has been radially discretized into two annular domains.

2.2.2 Effects of temperature distribution

As stated, the temperature feedback effect introduced by a temperature distribution within the reactor core is going to be investigated. The theory behind these topics have been previously discussed, providing a general overview of the thermal feedback effect and focusing the attention on the fast spectrum reactor cases.
The Serpent2 reactor core model must be properly modified in order to take into account the thermal expansion due to the change in density of the materials, as a consequence of the temperature distribution. As known, as its temperature increases, the material density tends to decrease: this physical phenomenon can be microscopically justified with the change in the random motion of material molecules, which affects the bond length of the material at equilibrium conditions.

Such processes can be modeled by knowing the temperature change and the thermal expansion coefficient, the temperature dependent material-specific value that describes the material response to the temperature gradient. In this work, some approximations have been made: neither superficial nor volumetric expansions have been evaluated but linear expansion is assumed in both the radial and axial direction of some assemblies' components: the fuel pellets, the stainless steel cladding and ducts, and the boron carbide neutron absorber pellets. The linear expansion coefficient for fuel, B4C and the stainless steel are listed in table 2.4.
For both the MOX and the B4C, which are present -respectively - in the fuel assemblies and in the control ones, with two different enrichment, the same thermal expansion coefficient is assumed, one for the fuel and one for the boron carbide, despite their different enrichment. MOX and lead's temperatures are set according to table 2.3, while the boron carbide and the stainless steel's temperatures are set to the average temperature between the fuel and the coolant. This implies that if the average temperature of these materials does not match the specific values listed in the table, a linear interpolation between the nearest listed temperatures is performed to determine the expansion coefficient. In addition, for those temperature sets whose average temperature is strictly higher than $T_m = 1073K$, the expansion coefficients associated to the neutron absorber and the stainless steel is set to last available value associated to the highest available temperature. This choice inevitably introduces some errors. However, due to the lack of tabulated data, it becomes necessary and can be considered acceptable, as the effect of the neutron absorber thermal expansion is certainly negligible compared to that of the fuel.

T [°C]	α_{MOX} [m/K]	α_{SS} [m/K]	α_{B4C}[m/K]
100	1.0528E-05	1.707E-05	0.4344E-5
200	1.0553E-05	1.740E-05	.4468E-5
300	1.0587E-05	1.774E-05	0.4588E-5
400	1.0631E-05	1.808E-05	0.4707E-5
500	1.0684E-05	1.841E-05	0.4826E-5
600	1.0747E-05	1.875E-05	0.4942E-5
700	1.0802E-05	1.908E-05	0.5058E-5
800	1.0889E-05	1.942E-05	0.5173E-5
900	1.0992E-05	-	-
1000	1.1116E-05	-	-
1100	1.1261E-05	-	-
1200	1.1429E-05	-	-
1300	1.1620E-05	-	-

Table 2.4: Linear Expansion Coefficient.

The automated procedure through which the Serpent2 geometry model gets modified has been implemented with an object-oriented code developed in Python3. The object-oriented code allows to build a system made by a collection of object, which - in this case - consist in a set of *classes* that provide an abstract definition of the real objects one want to model. A class instance is characterized by attributes and methods, which allows to modify the state of the class itself.
Therefore, in the main code three classes are defined:

- The *Material* class, which defines the material according to its temperature and density evaluated at 673 K and allows to import the new material temperature and evaluate its new density;
- The *Component* class, which initializes a component with an instance of the Material class. It defines the component through its default radial and axial dimensions, evaluated at 673 K and computes the new component dimensions;
- The *Lattice* class, which it is initialized with an instance of the Component class, and defines the new lattice pitch in between the pin tubes of an assembly.

Within the Material class, as said, the new density of the material is evaluated. With the exception for the coolant, whose density is computed through an empirical

equation provided by the ALFRED-NEA benchmark [5] (eq. 2.2, where T is expressed in Kelvin), for each other material the new density is defined as follows (eq. 2.1):

$$\rho_{new} = \frac{\rho_{old}}{[1 + \alpha \cdot (T_{new} - T_{old})]^3} \tag{2.1}$$

$$\rho_{Pb} = 11441 \frac{kg}{m^3} - 1.2795 \frac{kg}{m^3 K} \cdot T \tag{2.2}$$

For what concerns the computation of new dimensions, as mentioned before, some approximations have been adopted. Materials are assumed to undergo isotropic expansion: this allows to introduce a linear scaling factor (2.3), through which it is possible to compute the new dimensions values, supposing that the material keep its shape and uniformly expands in all three dimensions.

$$f_s = \frac{1}{\left(\frac{\rho_{new}}{\rho_{old}}\right)^{1/3}} \tag{2.3}$$

As regards the computation of the new triangular lattice pitch, the following formula has been implemented within the Lattice class definition:

$$p_{new} = p_{old} \cdot [1 + (R_{new} - R_{old})] \tag{2.4}$$

where R_{new} and R_{old} are defined as the ratio between the area of an elementary cell of the triangular lattice and the cross-sectional area of the pin times the total number of pins defining the lattice (eq. 2.5).

$$R = \frac{\frac{\sqrt{3}}{4} P^2}{\pi r^2 n_p} \tag{2.5}$$

2.2.3 Minicore strategy

In this paragraph some aspects regarding the reactions cross-sections evaluation are going to be discussed. The Serpent2 model previously described has been exploited either to retrieve reference parameters and quantities' distributions (the multiplication factor, the power and flux distributions) and to determine the group-wise reaction cross sections, collapsed over the fine energy grid structure.

At the beginning of this work, the transport model and the diffusion one have been tested with a coarser grid characterized by six groups, as it will further described. Such procedure has allowed to properly tune the neutron population parameters in order to obtain the nuclear data with an adequate statistics. The ultimate set of parameters are defined through the "set pop" card:

```
set pop 1500000 150 50 1.00000
```

whose values respectively represent the total number of simulated neutrons per generation, the total number of active cycles (which are the ones from which data are actually collected), the number of inactive cycles (which instead are needed to allow the fission source to converge) and the initial guess for the effective multiplication coefficient.
The complexity associated to this crucial step increases as one shifts towards finer energy grids, as a compromise between the computational time and the statistics associated to the computed results needs to be achieved. In the framework of this thesis work, the fine energy structure is composed by 37 energy groups, whose boundaries are listed in table 2.5.

Still keeping the population setting as it is, by increasing the number of groups, hence, by reducing the amplitude of the energy intervals, the statistics associated with the nuclear data worsen with a more or less significant trend, depending on the location of the universe within the system. In fact, the regions particularly subjected to this issue are the structural ones, in almost every type of assembly. Those regions are located in the bottom part of the ALFRED core and are, namely: the spike, the diagrid, and the lockage. Up to this moment, the reaction cross-sections associated with these regions have been evaluated though the full core model previously described. Such nuclear data are inaccurate from the point of view of their future application, being characterized by higher relative standard deviations (RSD). To be more specific, this problem involves the macroscopic cross-sections related to high energy groups: it is in fact true that the probability with which fast neutrons reach the structural and, in general, peripheral regions is very low in the framework of fast neutron reactors, as they tend to undergo fission in the *active* inner or outer region of the core.
This aspect is even more critical when one feeds these data to the diffusion code. To cope with this issue it has been decided to fed the FRENETIC code an hybrid

set of reaction macroscopic cross-section: every core region is associated with Σ_x coming from the full-core Serpent2 modeling but the aforementioned structural regions.

For those last ones it has been decided to build specific Serpent2 models, which are going to be referred to as "mini-core models", in order to improve the statistics of nuclear data. Mini-core models are characterized by an 5x5 hexagonal lattice, whose most significant feature is represented by the boundary conditions, which define the neutrons behavior as they cross the lattice boundaries. Such boundary conditions are intentionally set as "reflective" through the use of the "*set bc*" card, so that neutrons are forced to be reflected towards the inner region of the core through a coordinate transformation method, hence building up a three-dimensional infinite lattice structure.

Three different mini-core models have been defined: one for the inner fuel assembly only, one for the safety rods and one for both the outer fuel assemblies and the control rod (fig. 2.6), in order to take into account the full core arrangement of the assemblies. By looking at the radial view of the inner fuel assembly lattice, one senses that the model is not affected by the control rod position, as the the lattice does not include the CR at all. In principle, this could be an advantage since such macroscopic cross-section may be employed in the diffusion code, despite the arrangement of the control rods, if it is properly tested that the negative effects associated to this choice are negligible. This is all the more true, the lower the importance associated to the involved regions.

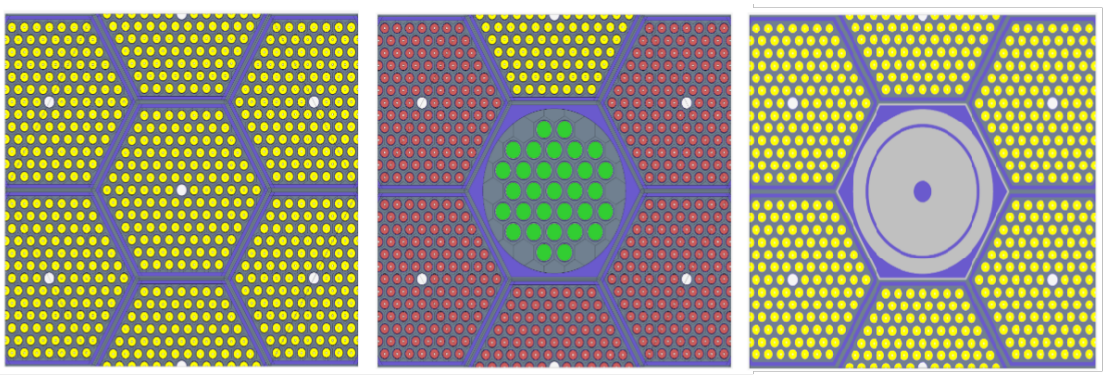

Figure 2.6: Mini-core radial view of the inner fuel model (left), the control rod and outer fuel model (center) and the safety rod model (right).

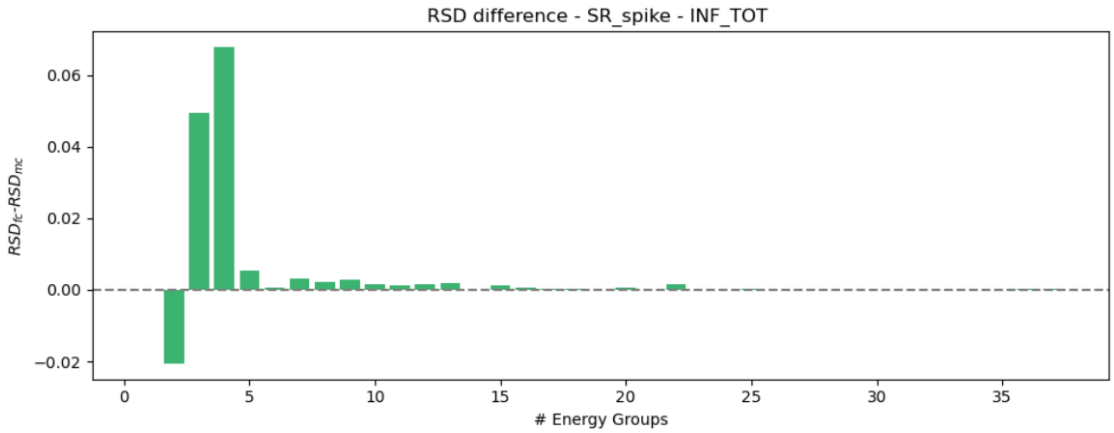

Figure 2.7: Σ_t RSD difference between full-core and minicore simulations for SR-spike structural region.

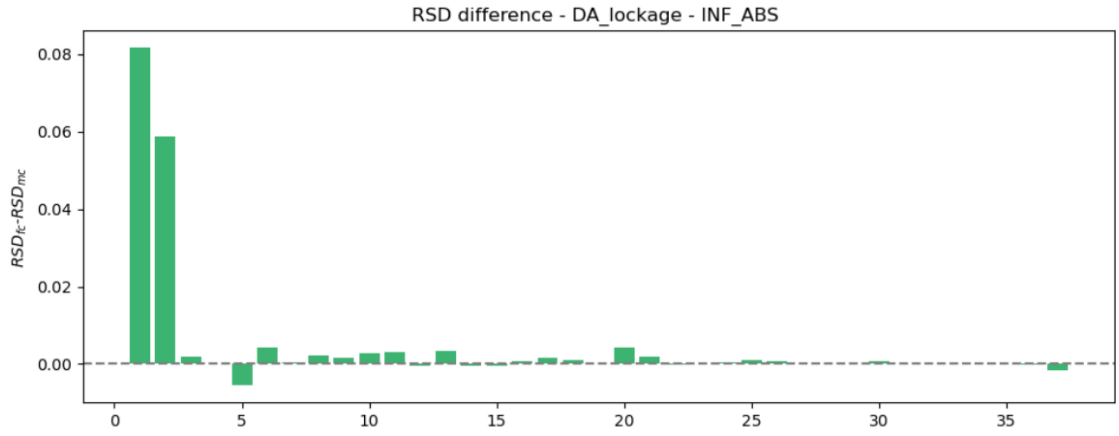

Figure 2.8: Σ_{abs} RSD difference between full-core and minicore simulations for DA-lockage structural region.

In figures 2.8 and 2.7 the absolute difference between some significant reaction cross-sections evaluated with full-core simulations and by applying the minicore approach are represented in the plots for two different structural regions belonging to two different types of assemblies, the safety assembly and the dummy one. Such plots allows to assess that, as correctly supposed, higher reaction cross-sections uncertainties are met for higher energy groups, as fast neutrons are more likely to get captured in the bulk region of the reactor instead of reaching regions far away from the active one. On the contrary, lower RSD are achieved for low energy

groups, as those neurons with a higher probability of reaching the structural regions are going to be slowed down along their path. Moreover, the graphs above also highlight that lower uncertainty are achieved by applying the minicore approach, as intended, because of the nature of the model itself, which does not allow neutrons to escape the domain. For the sake of completeness, the total macroscopic cross section trend and associated RSD, obtained by fullcore simulations and minicore ones, are depicted in figures 2.9 and 2.10.

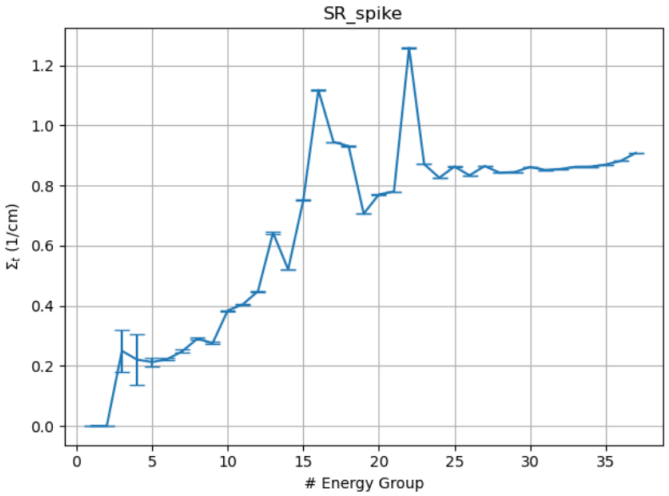

Figure 2.9: Σ_t from fullcore simulations for SR-spike region.

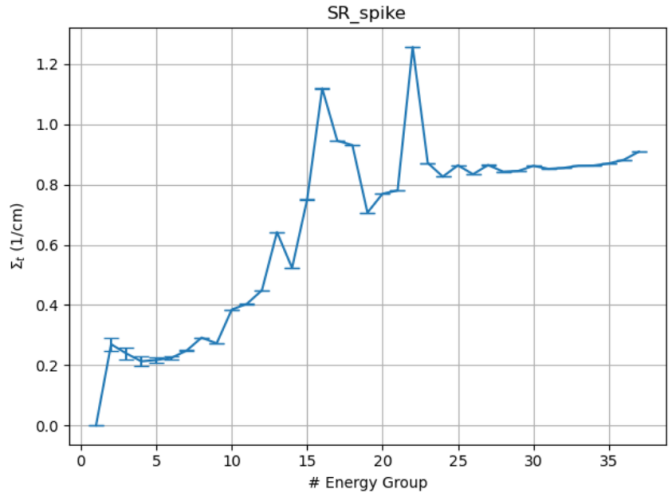

Figure 2.10: Σ_t from minicore simulations for SR-spike region.

Energy Group	Upper boundary (MeV)	Lower boundary (MeV)
1	20	3.678794E+00
2	3.678794E+00	2.231302e+00
3	2.231302e+00	1.353353e+00
4	1.353353e+00	1.108032e+00
5	1.108032e+00	8.208500e-01
6	8.208500e-01	4.978707e-01
7	4.978707e-01	3.019738e-01
8	3.019738e-01	1.831564e-01
9	1.831564e-01	1.110900e-01
10	1.110900e-01	6.737947e-02
11	6.737947e-02	5.516564e-02
12	5.516564e-02	4.086771e-02
13	4.086771e-02	2.478752e-02
14	2.478752e-02	1.503439e-02
15	1.503439e-02	9.118820e-03
16	9.118820e-03	5.530844e-03
17	5.530844e-03	3.354626e-03
18	3.354626e-03	2.034684e-03
19	2.034684e-03	1.234098e-03
20	1.234098e-03	7.485183e-04
21	7.485183e-04	4.539993e-04
22	4.539993e-04	3.043248e-04
23	3.043248e-04	2.039950e-04
24	2.039950e-04	1.486254e-04
25	1.486254e-04	9.166088e-05
26	9.166088e-05	6.790405e-05
27	6.790405e-05	4.016900e-05
28	4.016900e-05	3.051126e-05
29	3.051126e-05	2.260329e-05
30	2.260329e-05	1.370959e-05
31	1.370959e-05	8.315287e-06
32	8.315287e-06	6.160116e-06
33	6.160116e-06	4.000000e-06
34	4.000000e-06	2.360000e-06
35	2.360000e-06	1.370000e-06
36	1.370000e-06	5.400000e-07
37	5.400000e-07	1.0e-11

Table 2.5: EN37 energy grid employed as fine starting energy structure.

2.3 FRENETIC set up

Fast REactor NEutronics/Thermal-hydraulICs (FRENETIC) is a multiphysics computational tool who aims at simultaneously solving the neutronic and thermal-hydraulic equations both in steady-state and time-dependent conditions, at the full-core level of lead-cooled fast reactor core with the hexagonal fuel element configuration. This code has been developed at Politecnico di Torino in the last decades, being successfully validated [6] and hence providing a promising tool to characterize LFR in several core design configurations - but also in accidental scenario - with a very reduced computational time. The code implements a neutronic (NE) model and thermal-hydraulic (TH) one, which are coupled together to provide a multiphysics description of the LFR under investigation.
In the following sections, a concise but exhaustive description of both the neutronic and the thermal/hydraulic models is provided. In addition, an overview of the preliminary steps that has been taken to properly set up the diffusion code is given, as a correct and reliable configuration of the code strongly impacts the accuracy of the subsequent Genetic Algorithm optimization runs.

FRENETIC neutronic (NE) and the thermal-hydraulic (TH) models

The neutronic model governed by the steady-state or the time-dependent multigroup diffusion equation, which allow the module to return the neutron flux distribution and the thermal power. As this last formulation includes a time-dependent term - as opposed to Eq. 1.23 - it also accounts for the presence of delayed neutron precursors.

$$\begin{cases} \frac{1}{v_g}\frac{\partial}{\partial t}\Phi_g(\vec{r},t) = \nabla\cdot D_g(\vec{r},t)\nabla\phi_g(\vec{r},t) - \Sigma_{t,g}(\vec{r},t)\phi_g(\vec{r},t) + \sum_{g'}^{G}\Sigma_{sgg'}(\vec{r},t)\Phi_g(\vec{r},t) + \\ \\ +(1-\beta)\chi_{pg}(\vec{r},t)\Sigma_{fg}(\vec{r},t)\Phi_g(\vec{r},t) + \sum_{i=1}^{R}\chi_{dgi}(\vec{r},t)\lambda_i c_i(\vec{r},t) + S_g(\vec{r},t) \\ \\ \frac{\partial}{\partial t}c_i(\vec{r},t) = \beta_i\sum_{g=1}^{G}\nu\Sigma_{fg'}(\vec{r},t)\Phi_g(\vec{r},t) - \lambda_i c_i(\vec{r},t) \end{cases}$$

where g goes from 1 to G (total number of energy groups) and i goes from 1 to R (total number of delayed neutron precursors families). For the sake of completeness, D_g is the diffusion coefficient, χ_{pg} is the prompt neutron fission energy spectrum, χ_{dgi} is the delayed neutron fission energy spectrum associated to the precursor family i. β_i and λ_i are, respectively, the fraction of delayed neutrons and the decay constant associated to the precursor family i. As known, the total fraction of delayed neutrons is:

$$\beta = \sum_{i=1}^{R} \beta_i \tag{2.6}$$

The domain is discretized with a usually *coarse* mesh structure, which needs to be tailored according to the configuration of the reactor and the needs of the study. The requirement of identifying a properly coarse mesh comes from previous studies, which have highlighted the need of avoiding excessively optically thin regions that would affect the convergence of the method [7]. The application of nodal discretization results in the spatial homogenization of the material properties within each computational bin defined by the mesh. This means that, within each volume identified by the grid, the heterogeneous composition of materials is averaged, along with the all the nuclear data coming from the Serpent2 transport code. Since the multigroup macroscopic cross sections are also involved in this spatial homogenization process, the procedure is carried out according to the following formula [6]:

$$\overline{\Sigma}_{g,i} = \frac{\int_{V_i} d\vec{r}\overline{\Sigma}_g(\vec{r})\overline{\Phi}_g(\vec{r})}{\int_{V_i} d\vec{r}\overline{\Phi}_g(\vec{r})} \approx \frac{\sum_{i=1}^{N}(\overline{\Sigma}_g(\vec{r})\overline{\Phi}_g(r)h_{MC})}{\sum_{i=1}^{N}(\overline{\Phi}_g(r)h_i)} \tag{2.7}$$

where h_i is the axial length of the FRENETIC coarse grid and h_{serp} is the length of the j-th Serpent axial region which falls within the i_{th} axial mesh of FRENETIC, while N is the total number of materials localized in the i_{th} axial region of the FRENETIC mesh.

On the other hand, the thermal-hydraulic model solves the mass, the momentum and energy conservation laws for both the fuel and the coolant. Because of the weak radial thermal coupling between the adjacent fuel assemblies, the complexity of the problem is reduced by taking into account a set of weakly coupled one-dimensional problems, one for each sub-assembly.

$$\begin{cases} \frac{D}{Dt}\rho_c(\vec{r},t) = -\rho_c(\vec{r},t)\nabla\cdot\vec{u}(\vec{r},t) \\ \rho_c(\vec{r},t)\frac{D}{Dt}(\vec{r},t) = \nabla\cdot\hat{\sigma}(\vec{r},t) + \rho_c(\vec{r},t)\mathbf{f}(\vec{r},t) \\ \rho_c(\vec{r},t)\frac{D}{Dt}e_c(\vec{r},t) = \hat{\sigma}(\vec{r},t) : \nabla\vec{u}(\vec{r},t) - \nabla\cdot\vec{q_c}(\vec{r},t) + Q_c(\vec{r},t) \end{cases}$$

$$\rho_f(\vec{r},t)\frac{\partial}{\partial t}e_f(\vec{r},t) = -\nabla\cdot\vec{q_f}(\vec{r},t) + Q_f(\vec{r},t) \tag{2.8}$$

By simultaneously solving the one-dimensional set of equation governing the coolant flow Eq. 2.3 and Eq. 2.8 , which instead describes the heat conduction equation within the fuel , the model produces averaged values of the coolant and the fuel temperatures, along with the coolant velocity and pressure at each node. As anticipated, the one-dimensional channels are then weakly thermally coupled in such way to result in an approximated three-dimensional model that accurately describes the full-core thermal-hydraulic behavior of the system. The spatial mesh employed by the thermal-hydraulic model is usually coarser with respect to the one used in the neutronic model, which introduced two assumptions concerning the fuel and the coolant temperatures. The former requires that a single averaged temperature must be assumed to represent the temperature profile in each pin fo the neutronic mesh coordinate z_j, while the latter assumes that the Pb temperature

is averaged over the entire fuel assembly cross-section (x-y). Meaning that [6]:

$$T_{c,f}(z_j) = \frac{1}{L_h} \int_{z_j - L_h/2}^{z_j + L_h/2} T_{c,f(z')} dz' \tag{2.9}$$

where L_h is the z dimension of the neutronic model coarse mesh.
The actual coupling between the two module of the multiphysics code differs whether the simulation is performed in steady-state or time-dependent condition. In the first case, the coupling is given by an iterative exchange of data. Specifically, the neutron flux distribution computed by the neutronic module is provided to the thermal-hydraulic one in order to produce the temperature distribution. In turn, while the thermal-hydraulic supplies the new temperature profile back to the neutronic module so that the cross sections can be updated. If the simulation is performed in time-dependent condition, the neutronic and the thermal-hydraulic models are solved in parallel, and their outputs (respectively, the power and the temperature distributions) are exchanged.
The coupled approach is fundamental in order to address the effects of the thermal feedback on reactor's behavior and overall performances. It is in fact true that the macroscopic cross sections are strongly dependent on both fuel and coolant temperatures, as the change in temperatures affects the Doppler effect and, of course, the properties of the media.

With this intention, multigroup cross-sections at different temperatures for both the coolant and the fuel need to be generated by the Serpent2 Monte Carlo code, as already explained in the previous section, As indicated in [6], the feedback effect in FRENETIC is assumed to be a bi-variate linear interpolation on the cross section values:

$$\Sigma(T_c, T_f) = \Sigma(T_{c0}, T_{f0}) + \left(\frac{\partial \Sigma}{\partial T_f}\right)_{T_c} (T_f - T_{f0}) + \left(\frac{\partial \Sigma}{\partial T_c}\right)_{T_f} (T_c - T_{c0}) \tag{2.10}$$

2.3.1 Preliminary steps for FRENETIC core modeling

Among the preliminary activities needed for a proper modeling of the Lead-cooled Fast Reactor by the FRENETIC code, lies the searching of a proper axial mesh of the reactor assemblies. This procedure is not a trivial step, as the accuracy of

the FRENETIC outputs (with respect to the reference solutions computed by the Serpent2 Monte Carlo code) and the computational time strongly depends on the adopted axial space discretization.
In this framework, the effect on the computational effort, and hence the elapsed time, involved to retrieve the solution for each run is an aspect to pay particular attention to, as the Genetic Algorithm may probably investigate several hundreds of individuals for each reactor configuration. In addition to the ones aforementioned, several aspects need to be taken into account for the identification of a proper axial discretization, for example: the effect of material homogenization - as s result of the axial cuts definition - , the identification of properly optically thick regions, the spectral radius - hence the convergence rate - , etc. On top of those issues, the complexity of this step lies on the need of finding a proper axial discretization that performs sufficiently good for all the three reactor configurations under investigation (CR totally withdrawn, CR partially inserted and CR fully inserted): this would make possible to perform a consistent comparison among the outputs of the GA and, furthermore, to potentially apply the optimization code to transient cases. Because of this, a preliminary analysis on the effect of the discretization has been lead by using the macroscopic cross-sections computed by the Serpent2 code, collapsed over a six group energy grid (*PoliTO-LFR-6G*), whose energy boundaries are listed in table 2.6 .

Energy group	Upper boundary (MeV)	Lower boundary (MeV)
1	20	1.353
2	1.353	1.8316E-01
3	1.8316E-01	6.7379E-02
4	6.7379E-02	9.1188E-03
5	9.1188E-03	2E-05
6	2E-05	1E-11

Table 2.6: PoliTO-LFR-6G energy grid - group boundaries.

Another important criterion to mention is that the search for a proper axial discretization was driven by trying to maintain the distinction between the active regions of the fuel and control assemblies, rather than homogenizing them, and

by trying to preserve this aspect in all the three core configuration. Therefore, to better understand the choices behind the definition of the axial cuts, the heights of the active regions of the fuel assemblies and the control rod will be provided in table 2.7 and 2.8.

Fuel assembly	Lower boundary [cm]	Upper boundary [cm]
Inner fuel (MOX)	164	245
Outer fuel (MOX)	164	245

Table 2.7: Inner and outer fuel limits bottom and top elevations.

Control assembly	Lower boundary [cm]	Upper boundary [cm]
	CR withdrawn	
CRin90	74.5	119.5
CRin42	119.5	160
	CR partially inserted	
CRin90	106.5	151.5
CRin42	151.5	192
	CR fully inserted	
CRin90	161.5	206.5
CRin42	206.5	247

Table 2.8: CR absorber elevations.

Several spacial discretization have been tested, and the ultimate one

```
"zcuts":  [0, 61, 97.5, 106.5, 159, 164, 192, 245, 250, 263.5, 350],
"splitz":  [3, 2, 1, 3, 1, 3, 5, 1, 1, 4],
```

has the following impact on the simulations of the three core configurations:

Core configuration	k_{MC}	k_{FREN}	Δk [pcm]	**Elapsed time [s]**
CRout	1.07696	1.07887	-191	174
CRin0	1.05328	1.05329	-1	130
CRin55	0.999436	0.99503	439	104

Table 2.9: NE-module with PoliTO-LFR-6G.

The difference in the multiplication factor is defined as $\Delta k = k_{MC} - k_{FREN}$, so that it is possible to address whether the diffusion code overestimates or underestimates the quantity. It is worth to mention that the difference in the multiplication factor for the *CRin0* configuration is way too optimistic, leading to consider such value as a result of compensation errors. The compensation of errors can be attributed to numerical inaccuracies or limitation introduced by the algorithmic definition of the FRENETIC model with respect to the reference one, but may also be given by the employed energy grid or by the axial spacial discretization itself. For what concerns the energy grid, the effect is associated with the energy collapsing of the macroscopic cross-section that are going to define the dataset fed to FRENETIC, and this issue is going to be intrinsically treated in this thesis through the application of the GA, while the effect of the spacial discretization will not be investigated, being aware that it can be potentially approached through a genetic-based optimization.
The FRENETIC model setup appears in the following pictures, where the radial arrangement of the assemblies is depicted, as well as the ultimate axial discretization effect on the homogenization of the assemblies materials. In figure 2.11, information about both the geometry and the radial subdivision of the assemblies considered for generating the fine-group constants is shown . Indeed, the model developed in Serpent2 to obtained the cross-sections data for the neutronic diffusion simulations *only*, is not characterized by any radial discretization of the fuel assemblies, which is instead introduced for neutronic/thermal-hydraulic coupled simulations.

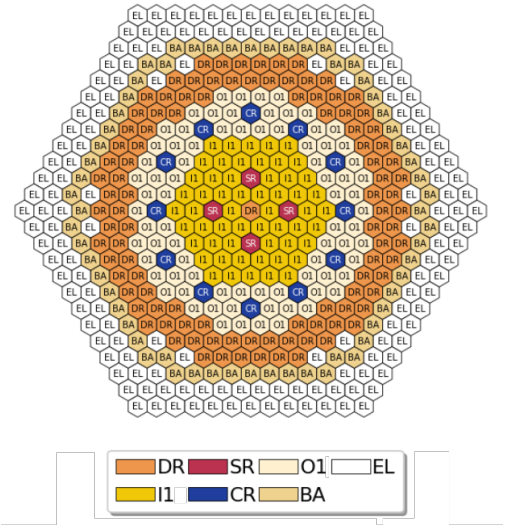

Figure 2.11: x-y view of the ALFRED core geometry.

Once defined the axial spacial discretization for the assembly, it has been applied to the same FRENETIC case. For each configuration the neutronic model has been called, provided with the nuclear quantities collapsed over the fine group energy structure, providing the results listed in Table 2.10.

Core configuration	k_{MC}	k_{FREN}	Δk [pcm]	**Elapsed time** [s]
CRout	1.09571	1.07887	-234	138
CRin0	1.07247	1.06913	-333	149
CRin55	1.01932	1.09336	-595	133

Table 2.10: NE-module outputs with EN37G.

In the following figures the difference and the percentage relative error between the radial total power distribution computer by the transport code and the one computed by FRENETIC by applying the fine grid is shown, for the three different core configurations. Both the quantities are plot so that it is easier to assess whether the diffusion code overestimates or underestimates the quantities themselves for each assembly.

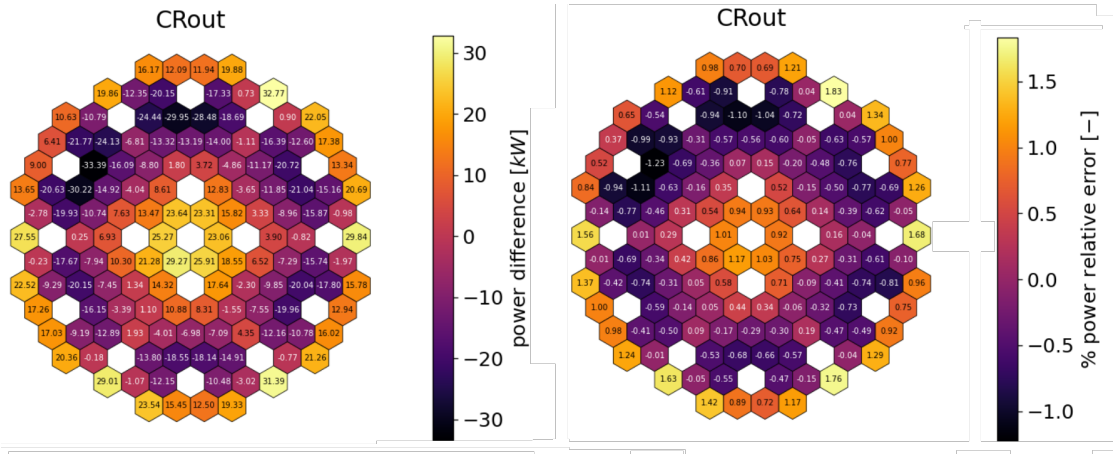

Figure 2.12: Power difference and percentage relative error for CRout.

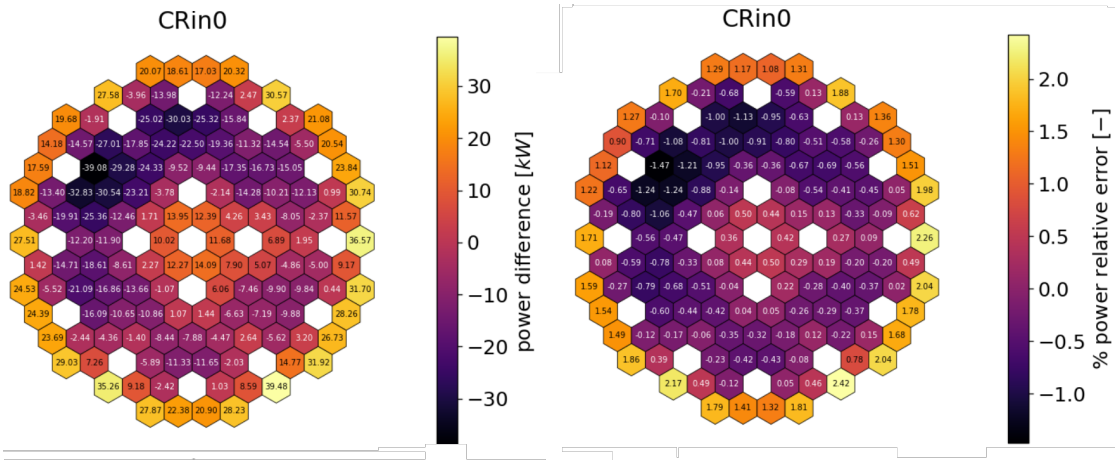

Figure 2.13: Power difference and percentage relative error for CRin0.

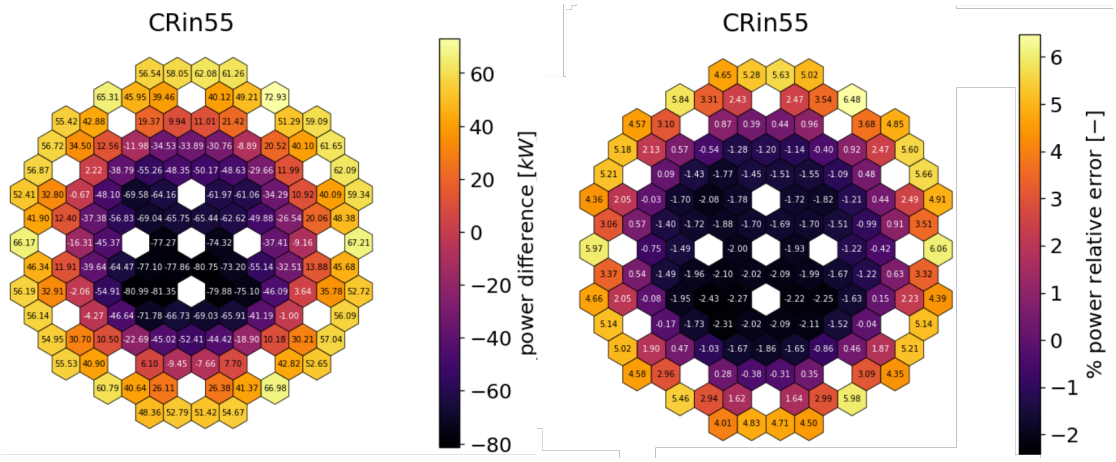

Figure 2.14: Power difference and percentage relative error for CRin55.

Chapter 3

The genetic algorithm

The identification of a proper energy group structure to collapse the nuclear data to be used in full-core simulations is a crucial step. The energy grid structure must be selected with the intention of preserving the physics of the problem, which is at the basis of accurate results, and to minimize as much as possible the computational effort involved in the simulation, both in the case of a transport model or a diffusion one. As these aspects are taken into account, the just named requirements are more likely to be met, the more optimal is the number of energy groups and their distribution along the energy axis: hence, the selection of an optimal energy grid structure has to be considered as a *stiff*, *non-linear optimization problem*, whose complexity increases as one moves toward fast spectrum systems.
In this framework, optimization techniques play a key role. Starting from a set of feasible solutions, optimization techniques aim at identifying the nearly-optimal solutions by using proper objective functions, which are usually maximized or minimized, according to their definition.
Evolutionary Algorithms (EAs) have been subject of research for more than thirty year: they are a class of computational methods that have been developed with the intention of mimicking the process of natural evolution, with the purpose of applying such evolutionary mechanisms to find approximated solutions for those complex optimization problems for which no exact solution method has been identified. Such algorithms are based on a collective leaning process within a population of individuals, which, taken together, represent the explored subset of potential

solutions in the solution space. There are three main streams that characterize the EAs: the *Evolution Strategies (ESs)*, the *Evolutionary Programming (EP)* and the *Genetic Algorithms (GAs)*, which differs one from each other in the representation of the solution, the processes that most affect the evolutionary process, the selection method and, of course, their applications.
Among these branches, GAs are the best known Evolutionary Algorithms,
Nowadays employed in a wide range of application fields, GAs started to be developed during the sixties by J.Holland, as a part of a study on adaptive processes - a system's ability to change and adjust itself as a consequence of the inputs received back by the environment. They are inspired by the biological mechanisms that govern the evolutionary processes: specifically, their working principle mimics the Darwinian mechanism underlying the natural selection. In this chapter, the Genetic Algorithm is introduced - as it is the tool employed in this thesis work for the automatization of the energy boundaries selection - with particular attention to the methodology underlying genetic-based optimization, the adopted chromosomal representation, and the choice of fitness functions.

3.0.1 Methodology of the genetic-based optimization

The GAs starts the optimization process by generating a set of N individuals, that constitute the initial population. The few-group energy structures of those initial solutions are guessed by the algorithm and strongly depend on the seed provided during the simulation setup. Each individual needs to be processed by the FRENETIC multiphysics code: the coupling between C++ and Python is needed, so that the few energy structure implemented in C++ for each individual is converted and given to the COREutils python package in order to collapse the group constants. After that, the input cases to be fed to the NE/TH modules are generated and the FRENETIC cases are processed. Following the simulation of all N cases using the diffusion code, the fitness functions are evaluated for each individual. These evaluations serve as the basis for assessing the performance of individuals within the generation, meaning that the definition of such operators, as well as the way they are combined, is a crucial step. Then a new generation is bred, taking into account some adaptive genetic operators that aim at generating new individuals in such a way to exploit and explore the solution space, also preserving

the best features coming from the best performing individuals. The steps briefly outlined here are iterated until a termination condition is reached. In this study there are four different stopping criteria that may end the evolutionary process: a specified tolerance on the combined FF value, a maximum simulation time, a maximum number of generations or a reached maximum number of inefficient ones, meaning that if the GA has not been able to update the best individual within a g_i number of generation, the search process is stopped. For the sake of simplicity, the workflow of the genetic-driven optimization process just described is depicted in figure 3.1, where the steps taken by the genetic algorithm itself are enclosed in the dashed box, and are implemented with a C++ language.

Stopping Criteria	
Max. generations	200
Max. inefficient generations	25
Max. time	500000
Min. joint FF	0.1

Table 3.1: Implemented stopping criteria for GA setup.

3.0.2 New generations breeding

As aforementioned, the new generation individuals must be bred so that two major aspects are addressed: the *exploitation* and the *exploration* of the solution space. Those two processes are extremely important to obtain a successful optimization of the problem. The former represents the process of visiting new regions of a search space, while the latter is the process of evaluating those regions of a search space within the neighborhood of good-performing individuals already explored in previous generations. Therefore, the genetic algorithm must provide a good balance between exploration and exploitation to be efficient and effective, and this is done by trying to correctly tune the *adaptive genetic operators*, which, in the case of this study, are defined a priori. It is generally assumed that the exploitation processes in EAs are performed by selection, while the exploration of new regions of the phase space is due to genetic operators such as *crossover* and *mutation*, even if many researchers have questioned this affirmation, also assessing that the

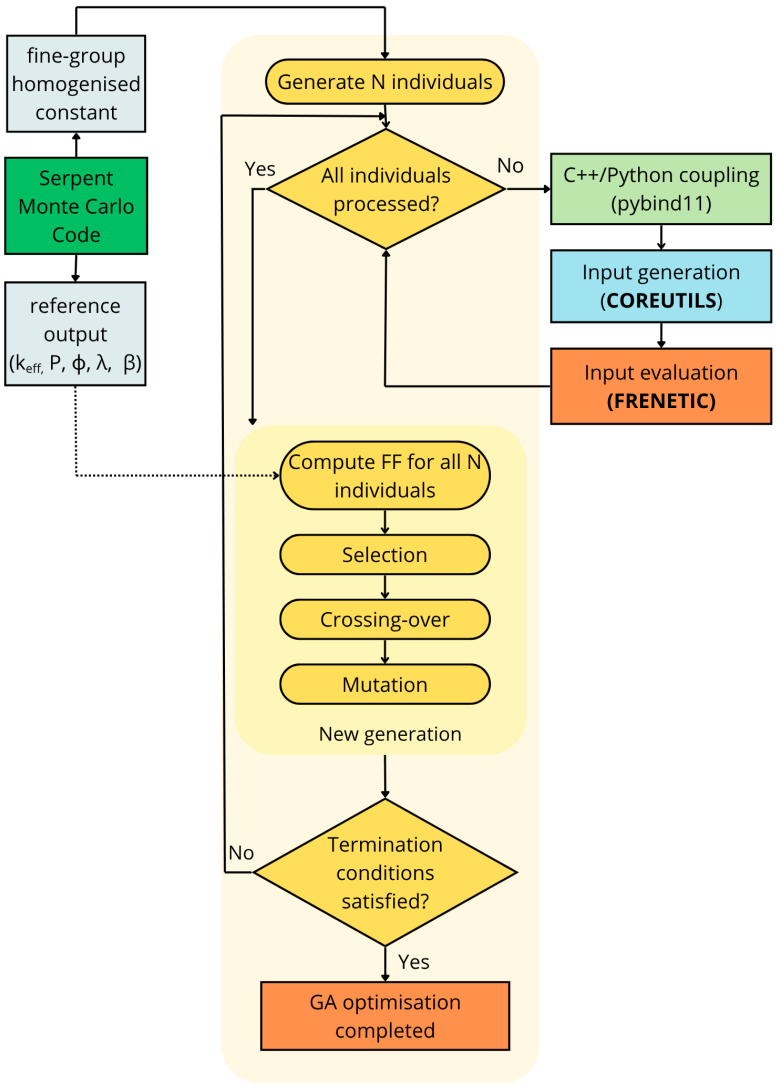

Figure 3.1: Workflow diagram of the GA optimization process [8].

influence of these adaptive genetic operators with respect to the exploration and exploitation process may also change according to the evolutionary strategy used in the study (i.e. EPs, ESs, GAs) [9]. An additional fundamental concept that must be introduced in the framework of evolutionary algorithms is the *selection pressure*, which refers to the intensity with which better individuals are favored for reproduction and survival in the coming generation. This aspect is of considerable

importance for determining the level of exploration or exploitation of the phase space: a higher selection pressure increases the emphasis on selecting the best-performing individuals of each generation, meaning that it pushes the algorithm to look for potential solutions in the neighbor of the current best-performing ones. This aspect may lead to a potentially faster convergence, but also to a risk of a poor exploration of the phase space and hence to the exclusion of potentially better performing individuals. On the other hand, the lower the selection pressure, the higher the diversity in the individuals of the population.

In this work, the new population is generated according to some non-adaptive rules, defined a priori. A certain amount of individuals comes from the *elitist selection* (f_E), the other one from *crossover* (f_{XO}). The remaining spots are instead destined to some randomly sampled individual coming from the previous generation: the random selection of sampled individuals allows to lower the selection pressure. Once the sample of individuals forming the new generation has been defined, each of them undergoes a certain probability of being *mutated*.
The elitist selection is a fundamental, if not essential, procedure in the identification of the new population, as it consists of preserving the top-performing individuals of the current generation by coping them with no alteration in the new one. Therefore, elitism must be perceived as an exploitation operator, as it helps to maintain a good quality of the solutions: the good features of the best-performing individuals are always inherited, speeding up the convergence, and lowering the probability of regression of the GAs. One drawback of elitist selection consists of the potential reduction of the genetic diversity. However, this issue is partially addressed by the mutation procedure, which randomly modifies some genes on the chromosome that defined the individual with a certain given probability. The recovery of the genetic diversity performed by the mutation operator allows one to explore new potential solutions, while still preserving most of the genetic material.
On the other hand, the crossover operator is responsible of the combination between two or more parent individuals. This operator is based on the assumption that combining the information coming from two individuals may generate better solution. To make sure that XO occurs, a mating pool from which couples of individuals are selected to originate a couple of offspring needs to be generated. The procedure through which the individuals composing the mating pool are

identified is the *tournament selection*. The individuals of the current generation are split into groups (tournaments) and ranked within the tournament itself. Each of the individuals is associated to a certain probability of being picked for XO and such probability lowers by $1 - p$ as moving toward less performing individuals. Grouping the individuals to perform localized ranking is a strategy to increases the survival probability of those individual with lower FF, which means that a direct relationship between the parameters of the selection method and the selection pressure exists and because of this it is possible to adequately tune the pressure itself. Additional information regarding the XO procedure is given in the following section, as it strongly depends on the way the chromosome is structured.

3.0.3 Chromosome structure

As well as for what occurs in biology, also in the contest of GAs the chromosome contains all the genetic information needed to define each individual of a population. The chromosome structure may vary depending on the study in which the GA optimization technique is applied, in order to more accurately represent the specifics of the problem. For what concerns this study, the only constraint in the definition of the chromosome structure is represented by the fact that the retained energy boundaries defining the individuals, hence appearing in the coarse energy grid, must correspond to the ones of the fine-groups energy grid structure given as input. In previous work an additional constraint was also taken into account, consisting in defining a priori the number of groups to collapse the nuclear data in. In general, this choice led to the limitation of the explored phase space, thereby excluding potentially high performing solutions characterized by a different number of energy groups.

The chromosomic representation employed in this study is inherited from [8], where more than one chromosomic definition have been tested, and the one used in this thesis comes out from a combination of their best features. Inspired by the biological condition of the polyploidy, this chromosome representation is an extension of the standard modeling of individuals. The karyotype - the set of chromosomes defining the individual - is composed of two chromosome: γ_0 and γ_1. The former, γ_0 is an haploid chromosome, composed by a single gene, which assumes an integer value $G \in \{1, H-1\}$, describing the number of *internal* energy

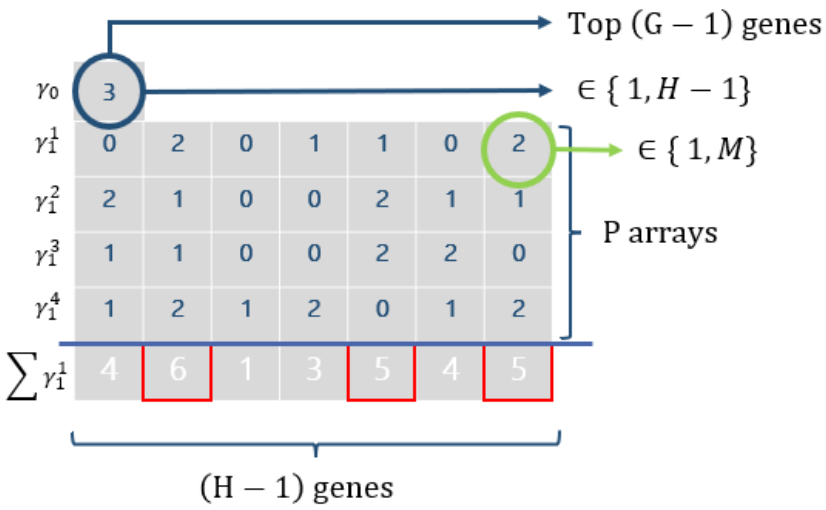

Figure 3.2: Chromosome representation [8].

boundaries of the coarse mesh. The latter, γ_1, is instead a polyploid chromosome. Therefore, it is actually made up of a *set* of chromosomes, consisting in P arrays each one with *H-1* number of genes. Each gene is associated with a possible energy boundary of the fine energy grid. Being H the number of groups of the fine energy structure, it can be inferred that the external boundaries of the grid are taken into account by default. Polyploid chromosome genes may assume an integer value in between the interval $0, M$, where Mdefined by the user. The resultant γ_1 chromosome that identifies the retained energy boundaries comes from the sum of the P arrays. The sum of the gene values actually allows to perform a ranking between the energy boundaries, hence the G number of chosen energy boundaries are the ones with the highest score. For what concerns the XO operation, the mixing of the genetic material is performed as follows. The offspring is not generated through a one-point crossover [10] but one of the P arrays of the γ_1 chromosome is randomly picked and entirely replaced by the one coming from the partner, therefore changing the resultant scores of the genes.

3.0.4 The fitness functions

The identification of proper fitness functions to be employed in genetic-driven optimization is a crucial step, since they define the required properties of the solution space. Moreover, since the evaluation of the fitness function is usually computationally expensive, a compromise between how computationally demanding the FF is and how accurately it reflects the quality of the solution must be achieved. In previous works developed at Politecnico di Torino [8], three different specialized fitness functions have been defined. The first fitness function consists in the absolute difference, expressed in *pcm*, in between the effective multiplication factor of the individual studied by the GA (k^I) and the reference value for the effective multiplication factor (k^{MC}), deriving by the Serpent full-core Monte Carlo simulation.

$$f_k^I = |k^I - k^{MC}| \times 10^5 \tag{3.1}$$

This first fitness function is very simple and very reliable, as it both demands a lower computational effort and it globally and effectively describes the state of the finite multiplying system under investigation. The second fitness function is defined for the power, and it actually consists in the relative error between power vectors computed with FRENETIC and Monte Carlo:

$$f_P^I = \sqrt{\sum_{j=1}^{J} \left(\frac{P_j^I - P_j^{MC}}{P_j^{MC}} \right)^2} \tag{3.2}$$

The last fitness function is a weighted relative error between the flux vector computed with FRENETIC and the Monte Carlo. For the sake of consistency, the flux coming from the transport code is collapsed on the same grid used in the individual under evaluation.

$$f_\Phi^I = \sqrt{\sum_{g=1}^{G} \sum_{j=1}^{J} w_{g,j} \left(\frac{\Phi_{g,j}^I - \Phi_{g,j}^{MC}}{\Phi_{g,j}^{MC}} \right)^2} \tag{3.3}$$

Different definitions of the weights have been tested in previous work [8]. The one preferred, and hence the one used in this project as it has a strong impact on the

convergence trend, exploits the the product of the adjoint times the neutron density, which actually represents the total importance in the phase space $(\vec{r}, E)$. Being aware of the relationship that exists between the direct and adjoint operators, it can be proved that the value of the total importance integrated over the whole phase space is constant in time. Meaning that the weight are defined as:

$$w_{g,j} = \frac{\psi_{g,j}}{< \psi >} \tag{3.4}$$

and hence they are constructed so that they are normalized:

$$\sum_{g=1}^{G} \sum_{j=1}^{J} w_{g,j} = 1 \tag{3.5}$$

As supported by previous work, the choice of this specific definition of the weights strongly affects the convergence speed of the optimization process. In addition, this formulation also allows to preserve important physical aspects, as it tends to mitigate the relevance of regions characterized by a high importance but a low neutron density.
In this thesis, the aforementioned fitness functions will be employed by the genetic algorithm (GA) in its attempt to simultaneously find a near-optimal energy grid for three different configurations. With respect to previous work, as follows the fitness functions related to kinetic parameters are going to be introduces and taken into account during the optimization process. Also in the future perspective of applying the GA in time-dependent simulations, the delayed neutron precursors will play a key role in the determination of the nuclear reactor system.
To provide a brief overview, fission reactions result in the direct emission of prompt neutrons and the indirect emission of delayed ones, with a certain fraction. The delayed neutrons originate from fission fragments, which are themselves products of the fission process. These fragments, known as *delayed neutron precursors*, undergo *beta decay* after a characteristic lifetime (*effective life-time,* Λ). If the nuclei undergoing beta-decay are highly excited, they may emit a neutron.
Hence, because of the role played by the delayed neutrons in time-dependent simulation, it would be useful to investigate the performances of the GA also taking

into account the effective delayed neutron fraction and the effective lifetime. As follows, the definition of the fitness functions, respectively:

$$f_{\beta}^{I} = |\beta^{I} - \beta^{MC}| \times 10^{5} \tag{3.6}$$

$$f_{\Lambda}^{I} = \frac{|\Lambda^{I} - \Lambda^{MC}|}{\Lambda^{MC}} * 100 \tag{3.7}$$

Some FFs are subjected to a control before being definitively assigned: in between them, the one related to the effective multiplication factor. There are several parameter that may influence the value of k_{eff} evaluated through the diffusion code, to name one, the axial discretization, that strongly affects the homogenization between the materials. It is possible that the absolute difference between the $k_{eff,FREN}$ and the reference one may be very small, approaching values around *1 pcm*. This outcome does not define the accuracy of the FRENETIC results, since it may be given by compensation errors. As a consequence, in order to try to avoid that very small values of $f_{k_k^I}$ could influence the optimization process without providing any further improvement, the choice applied in previous works (***ref abrate) to artificially assign a value of *10 pcm* to the associated fitness function, whenever it was less than *10 pcm*, has been retained. To justify this choice let's also recall that the effective multiplication factor, that can be mathematically obtained through the six factor formula, is a quantity that instantly defines the status the a multiplying system, from a global perspective. Also f_{Λ}^{I} is subjected to a control, being set equal to *10 pcm* whenever it assumes values lower than the threshold (10 pcm). For the same reason, when $log(f_{\phi}^{I}) < 1$, f_{ϕ}^{I} is set equal to the unit value, otherwise $f_{\phi}^{I} = log(f_{\phi}^{I})$.
On the other hand, if the value associated to any fitness function is too high, making the associated individual unacceptable from the point of view of the accuracy, the same FF are set equal to an infinite value. In this way the GA is able to reject these solution, so that they do not impact on the evolution.
The parameter responsible for determining the ranking of each individual performance within the population is the joint fitness function (joint FF). This function can be defined in various ways depending on the specific goals of the optimization process, but mostly on the basis of the definition of the single fitness function

themselves, and the physical meaning they hold. However, its general purpose is to provide a unified criterion that simultaneously considers all the fitness functions computed for each individual, thereby enabling a comprehensive comparison between the individuals that accounts for multiple aspects at once.
As well as for what has been already applied in previous work, the fitness function that governs the evolutionary process is given by a combination of the effects on the computed single fitness functions. Since the objective of this work is to identify a suitable energy structure to be shared between the three different reactor configurations, all the 15 FF (5 for each configuration) are taken simultaneously, evaluating the product between them. Because of the nature of these FF, they appear to differ not only in their orders of magnitude, but also in terms of the range of variability. This makes it necessary to properly manipulate these functions so that they become as comparable as possible. Hence, each FF undergoes a linear scaling, which allows to normalize each value with respect to the maximum and the minimum values of that FF evaluated up to that moment. Since the minimum and the maximum values may be updated during the evolutionary process, this step is to be considered dynamic, and consequences associated to this aspect needs to be taken into account. Moreover, this method implies that FF characterized by a limited range of variability affects the evolutionary process more than theoretically justified. The linear scaling can be expressed through the following operator, while the joint FF is defined in equation 3.9

$$h_L : f \rightarrow 1 + 99 \cdot \frac{f - min_{\forall I \in E}(f^I)}{max_{\forall I \in E} - min_{\forall I \in E}} \tag{3.8}$$

$$FF^I = h_L(f_k^I) \cdot h_L(f_P^I) \cdot h_L(f_\Phi^I) \cdot h_L(f_\Lambda^I) \cdot h_L(f_\beta^I) \tag{3.9}$$

3.0.5 Genetic Algorithm setup

Once discussed and defined the most important features of the GA employed in this study, some additional parameters for the upcoming optimization processes need to be set up. As previously mentioned, the initial guess of individuals strongly depends on the seed used to identify each *tribe*. Since this set of starting solutions has a significant impact on the subsequent stochastic optimization process, it

becomes necessary to test a minimum number of input strings (seeds). Therefore, in the following section, results are discussed for four different tribes, each one associated with a specific seed, and thus identified as: *Boltzmann*, *Fermi*, *Henry*, and *Bohr*. The tribe differ one to each other just because of the initial guess, while the termination conditions remain the same (Table 3.1). Also the parameter associated to the mutation, elitism and crossover laws are shared between the tribes, and are listed in Table 3.2.

Parameters	
Selection method	Tournament selection
Tournament number	10
Tournament probability, p	0.2
Mutation probability	20 %
Elitism fraction	10 %
Crossover fraction	20 %

Table 3.2: Parameters for GA setup.

In order to better understand the behavior of the GA in its attempt in finding a proper shared energy grid structure, it appeared intuitive to apply the same optimization algorithm to each core configuration taken by itself, so that it is easier to appreciate the impact of simultaneously take into account more than one configuration. A single tribe, *Boltzmann*, has been explored for the single-configuration runs, as the aim of this comparison is to try to highlight how different the best individuals are, in between a single-configuration case and a multi-configuration one, and also how the solution space changes has the number of reactor layouts to be simultaneously taken into account increases.
In these lines it is also anticipated that two different set of simulations have been performed for each multi-configuration tribe and for each single-configuration, which differ in the number of individuals constituting the single generation. This means that the number of individuals making up the initial population is increased from 50 to one hundred.

Chapter 4

Results discussion

In this chapter the collected results coming from the evolutionary optimization processes are presented: the differences between the single-configuration and the multi-configuration cases are highlighted, trying to provide a critical interpretation of the genetic algorithm outputs.

The following results are all based on the same set of parameter, which has been already discussed in the previous section. As anticipated, the chromosome representation is defined such that the minimum and maximum number of groups making up the coarse grid is defined a priori. These parameters have been respectively set equal to 4 and 20, hence limiting the solution space. This choice comes from previous studies [8] which have highlighted that in optimization processes involving a single core layout, solutions characterized by a number of energy groups higher than 20 do not survive the evolutionary process, due to their low chances of ranking among the best-performing individuals. This choice not only allows to preserve the hypothesis of the diffusion theory, but also meets the need of trying to reduce as much as possible the computational time, as the higher the number of groups the bigger the computational effort involved without an effective improvement in the accuracy of the results.

4.1 Isothermal reactor simulations

In this section of the chapter we are going to discuss the results coming from simulation in which isothermal conditions of the reactor are considered, setting the fuel temperature and the coolant one equal to $673K$.

4.1.1 Single core layout simulations results

The optimizations of the single core layouts have been conducted with the aim of identifying potential variations in the behavior of the genetic algorithm when three different reactor configurations are considered simultaneously. For the sake of simplicity, the displayed results are those coming from the simulations with a higher number on individuals per generation. The graphs that follows allow to observe how much the solution space (in general the number of groups and selected energy boundaries) changes considerably depending on the case under investigation. This aspect is encouraging, as underlines the Genetic Algorithm abilities in valuing the unique issues related to a specific problem, providing tailored solutions.

In Fig. 4.1 the trends of the joint FFs for each CRs position within the core are shown. From a preliminary analysis of the charts , one can observe how the nature of the individuals making up the first population impacts on the evolutionary process of the algorithm. This aspect can get noticed by looking at the average joint FF peaks reached at the beginning of the optimization process, for each simulation. As a consequence, the loss of some energy boundaries of the fine-grid is probably due to the individuals tested in this generational interval. This interpretation is also confirmed by the graphs in Fig. 4.4, which instead represent not only the positioning of the best individuals in the genealogical line, but also the evolution of the solution space from the point of view of the energy boundaries considered by the GA. Indeed, it is possible to observe that after roughly a thousand individuals, for the CRin55 case, and 500 individuals, for the CRout and CRin55 cases, the potential associated with some energy boundaries decreases. In certain cases, those boundaries are permanently disregarded, whereas in others, they may eventually re-emerge, most likely as a result of the cross-over and mutation processes.
An additional aspect to be noticed is that the three optimization processes show an encouraging trend of the average joint FF value, which rapidly decreases within a

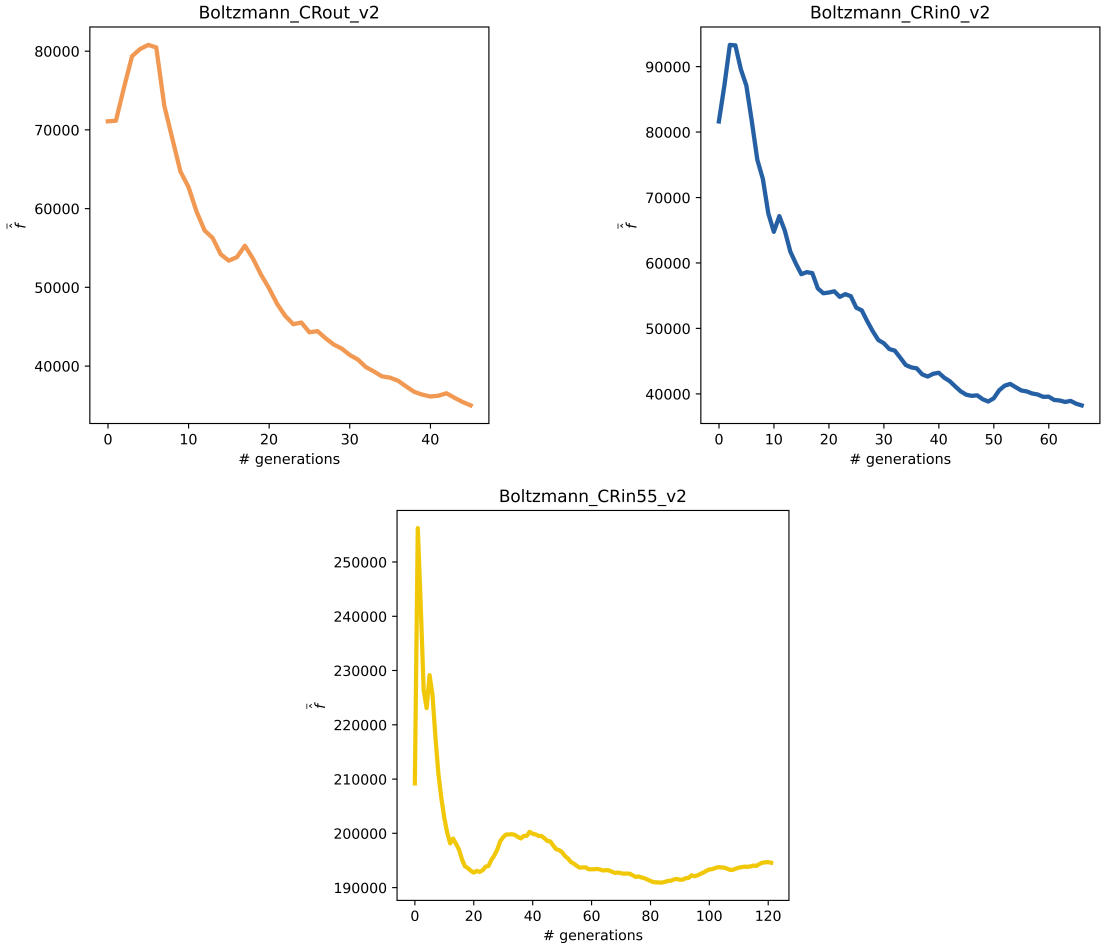

Figure 4.1: Average joint FFs trends over the number of generation.

few tens of generations and still get minimized as the generations increase, even if with a slower convergence speed. Moreover, in some cases (*CRin55*) the $\overline{\hat{f}}$ also seems to start fitting within a certain range. Still looking at Fig. 4.4, charts indicate that the stopping criteria to terminate the simulations has been the maximum number of inefficient generations, meaning that additional good performing individuals may still be identified by changing the stopping criteria and tolerating longer simulation times.

Instead, the charts collected in Fig. 4.2 depict how the number of energy groups constituting in the coarse energy structure are distributed among the individuals. It is possible to notice how, right after a fair number of generations, the algorithm has

already pushed the individuals towards a certain range of number of energy groups, the one that seems to give back more accurate results. The latest generations do not seem to deviate from this range, rather they exploit this data to explore potentially more performing individuals. It is also interesting to note how the number of groups preferred by the GA changes considerably depending on the position of the control rods inside the core. In Fig. 4.3 the energy structure of the best individuals is depicted with respect to the distribution of the energy-wise power, while the FF functions associated with these individuals are listed in Table 4.1.

BEST INDIVIDUALS			
	CRout	**CRin0**	**CRin55**
f_ϕ (%)	9.80	9.61	1
f_P (%)	0.240	0.517	0.640
f_Λ (%)	0.0278	0.024	19.168
$f_{k_{eff}}$ (pcm)	42.9	10	431.7
f_β (pcm)	10	10	49.8

Table 4.1: Best individuals output for single core layout simulations.

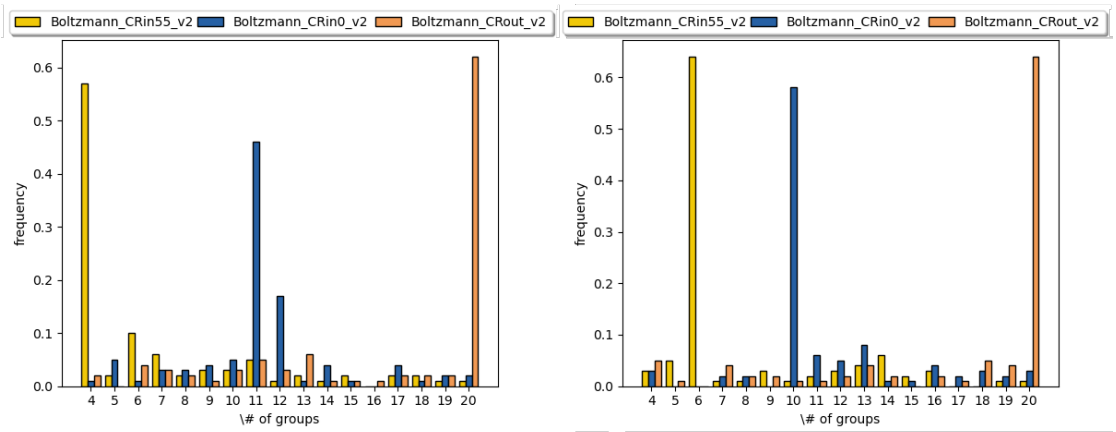

Figure 4.2: Distribution of individuals per number of groups at the 40^{th} generation for each core layout (left) and at the last generation of each core layout (right).

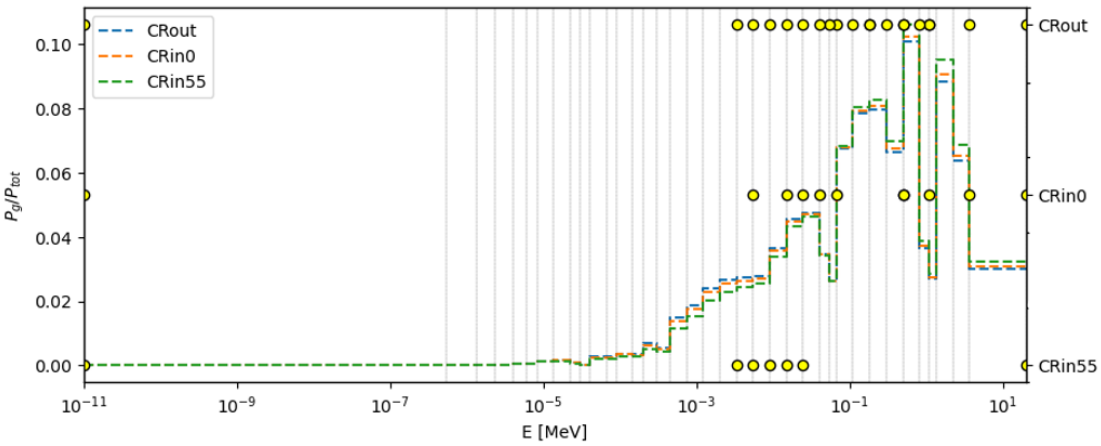

Figure 4.3: Best individuals of single configuration over power produced as a function of incident neutron energy. The dots represent the best individuals energy boundary for each configuration.

The lowest number of groups are met for the *CRin55* core configuration (the one with the CR fully inserted), and they are arranged in such way that two major groups can be identified, one involving thermal energies and energy groups up to 10^{-3} MeV, and one collapsing the high energy groups, from roughly 10^{-1} MeV up to 20 MeV. The higher energy discretization is met in the epithermal region. This energy groups distribution could be physically explained by considering the effect of the control rods themselves, which, when fully inserted, lead to a significant deformation of the neutron flux. A possible justification may be that for this reason, the Genetic Algorithm tends to create an energy group discretization in the energy range affected by the CR poisoning, obtaining more potentially robust homogenized cross sections, increasing the accuracy of the calculations. Practically, this allows to reduce the error associated with the neutron flux: in fact, the f_ϕ turns out to have a predominant effect, shifting the interest towards energy grids with a very low number of groups. On the other hand, the effect of f_ϕ does not seem to be particularly relevant in determining the coarse grid for the *CRin0* and *CRout* core configurations, whose best individuals are instead characterized by a higher number of energy groups, respectively 9 and 16. Indeed, the scaled f_ϕ for those two configurations are characterized by a very narrow range of variability, with values not falling below a specific higher one, with the exception of some individuals,

not statistically relevant, for which low values of the f_ϕ are reached with a small number of energy groups. Instead, the fitness function that seems to reflect the ultimate choice of the number of groups is the one associated with the effective multiplication factor. Also the fitness functions associated with β and Λ seems to be responsible for the ultimate number of groups, even if, despite their maximum value, the range of variability is limited. Quite the opposite, in the core layout with the CR fully inserted, f_β and f_Λ act in contrast with the behavior of $f_{k_{eff}}$, indeed, they are minimized with a higher number of the energy groups (with respect to the best performing individuals), also stating the higher importance of the f_ϕ discussed before. It is useful to highlight the fact that the fitness functions associated with those quantities may assume a different role while performing genetic optimization of a time-dependent full-core cases. The mentioned effects of the single FF can be appreciated in the graphs collected in Fig. 4.5.

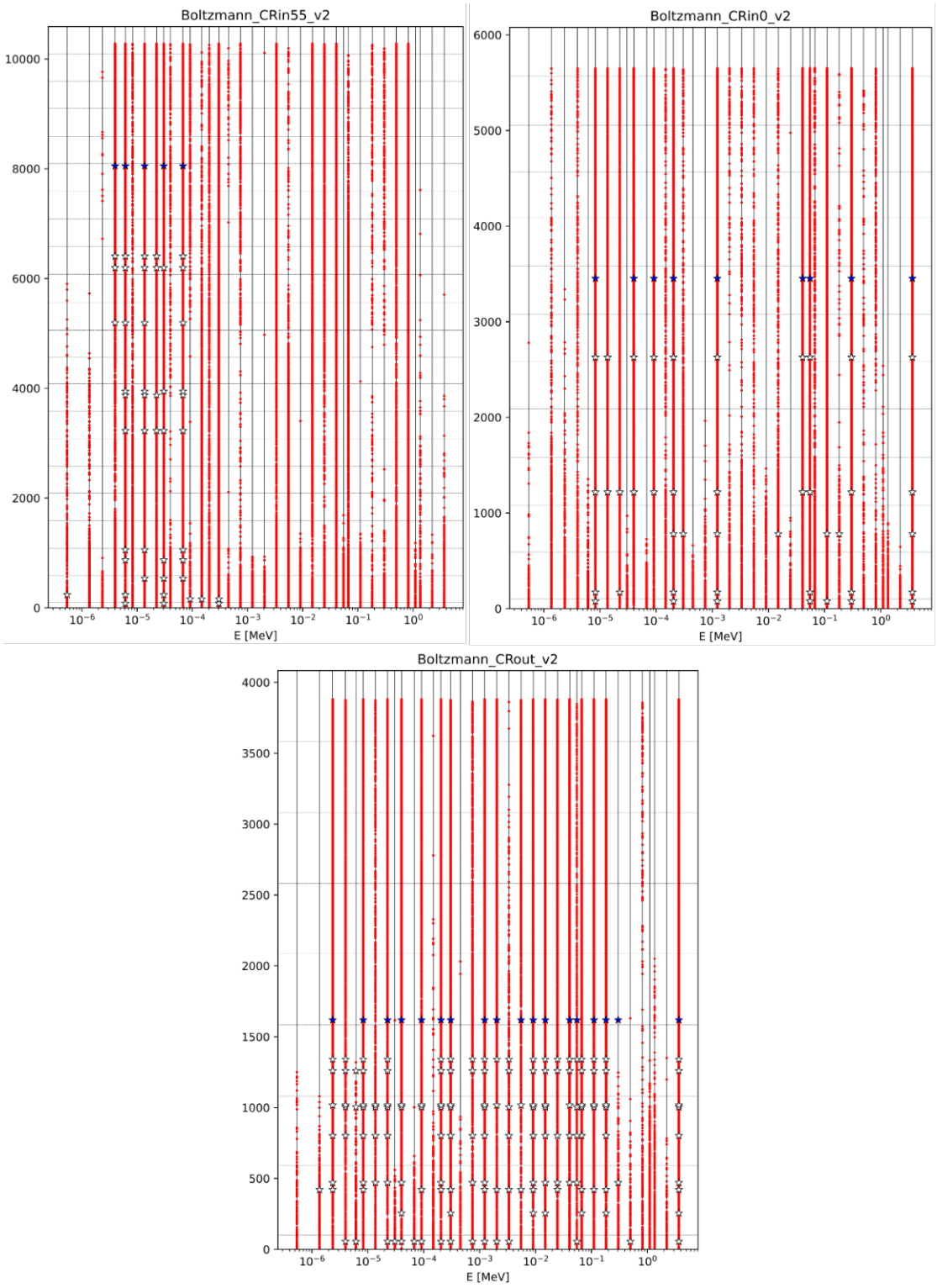

Figure 4.4: Evolution of the individuals per core configuration belonging to Boltzmann tribe. The vertical lines represent the starting fine energy structure, the red dots the individuals in each generation, the white stars indicate the best individuals energy boundaries while the blue stars the best individual.

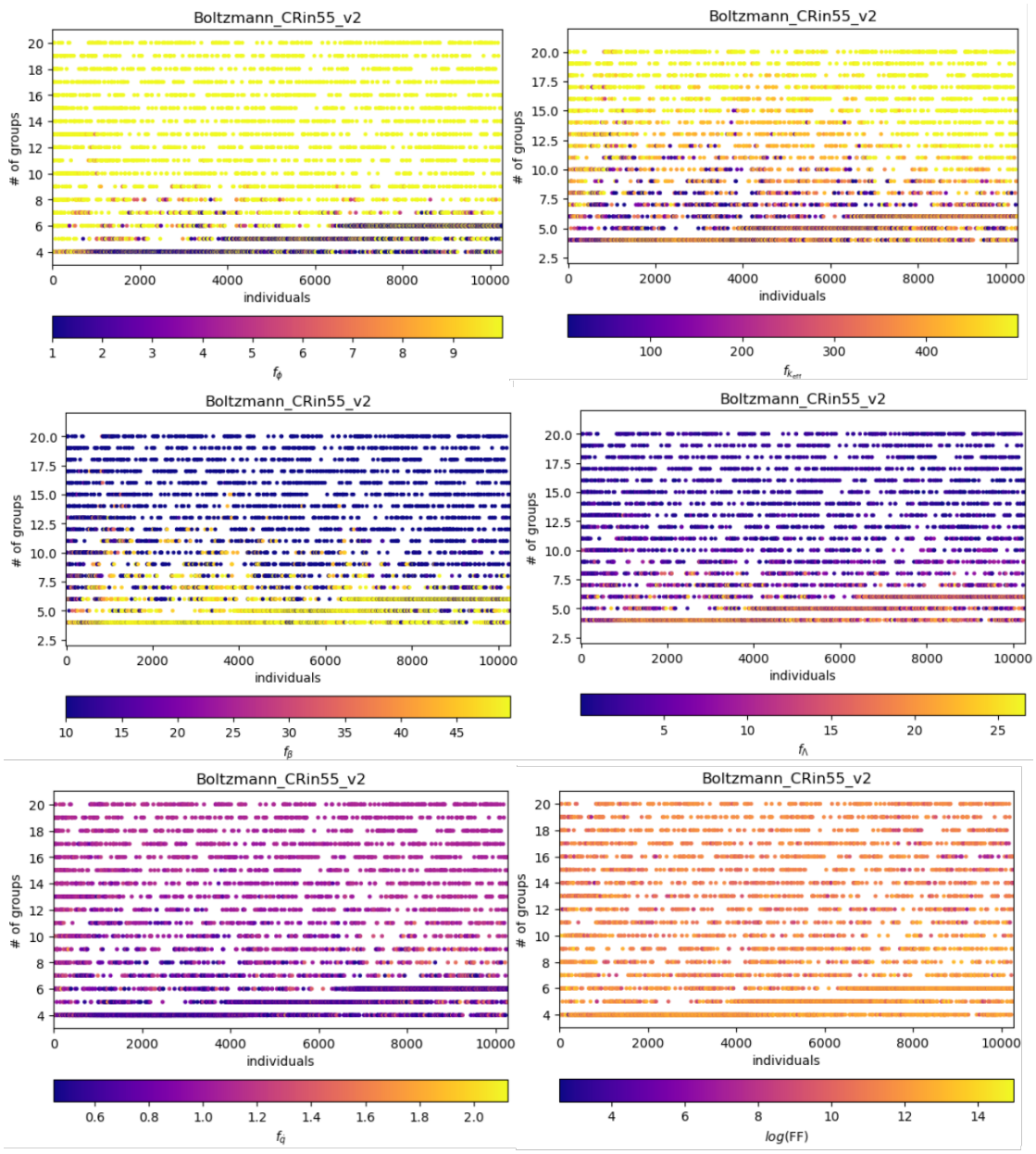

Figure 4.5: Fitness functions associated to the CRin55 configuration. FF of the flux (top left), k_{eff} (top right), β (middle left), Λ (middle right), power (bottom left) and their combination (bottom right). The dots represent all the individuals tested by the GA.

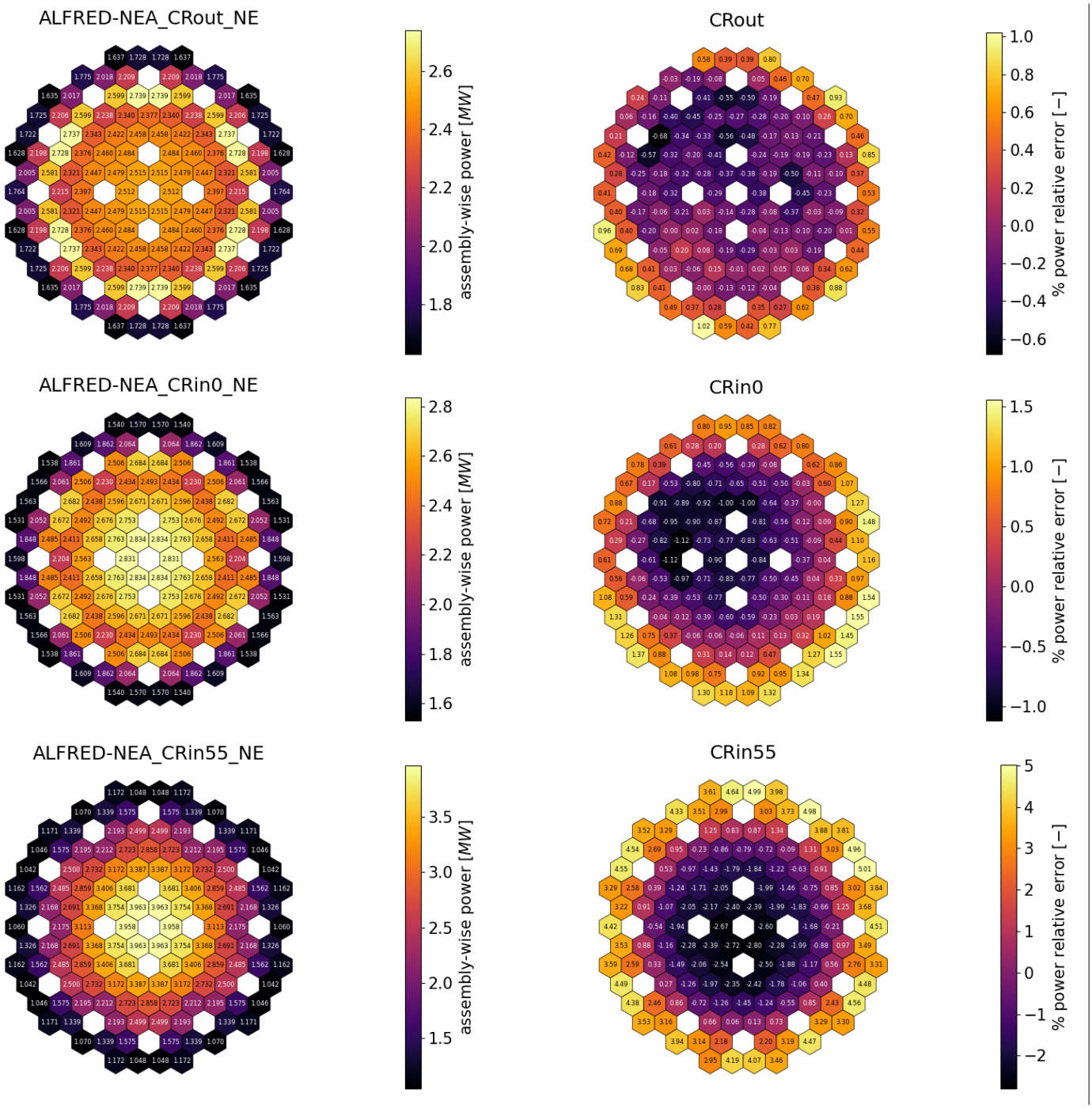

Figure 4.6: Best individuals from single configuration optimization processes. Radial power distributions (left) and power relative error with respect to Serpent2 (right) are depicted for each configuration.

4.1.2 Multi-configuration simulations results

The multi-configuration optimization processes have been testes changing the number of individuals constituting the initial population. The main differences in between those two sets of results are going to be highlighted in the following. As anticipated, a starting set of optimization processes involving four different seeds have been simulated, with a number of individuals per generation equal to 50. The same processes have been repeated doubling the initial population, while keeping unchanged the other setting parameters (Tab. 3.2). It has been noticed that despite increasing the number of individuals per generation, the computational time to perform the energy grid optimization and the total number of tested individuals are roughly the same, as a faster convergence is met. The convergence criteria are is reached in roughly half the number of generations. This feature seems to be shared by the seed-based simulations, despite their evolution trend at the beginning of the optimization process. On the contrary, with a limited initial population, the four simulations exhibited different convergence trends from one another, meeting the stopping criteria at distinct stages throughout their evolution. This aspect could suggest that an increased number of individual per generation seems to slightly reduce the dependency over the initial pool of individuals and, hence, on the input seed: indeed, the higher the initial population, the more homogenized the distribution of individuals among the number of groups. This aspect is supported by Fig. 4.9, where the initial distribution (0^{th} generation) has achieved a clearly more uniform distribution simply by doubling the individuals per generation.

Since the convergence of the joint FF is reached within a relatively small number of generations, the GA does not seem to be able to update the best individuals, which are identified within the first 15 generations, interrupting the optimization process for the reached maximum number of ineffective generations. This behavior explains the unexpected and limited total number of individuals tested by the tribes. In any case, the constraint imposed on the genetic algorithm (the requirement to identify a single energy grid which is *simultaneously valid* for three distinct configurations) represents a non-negligible limitation, as it likely imposes a significant restriction on the solution space.

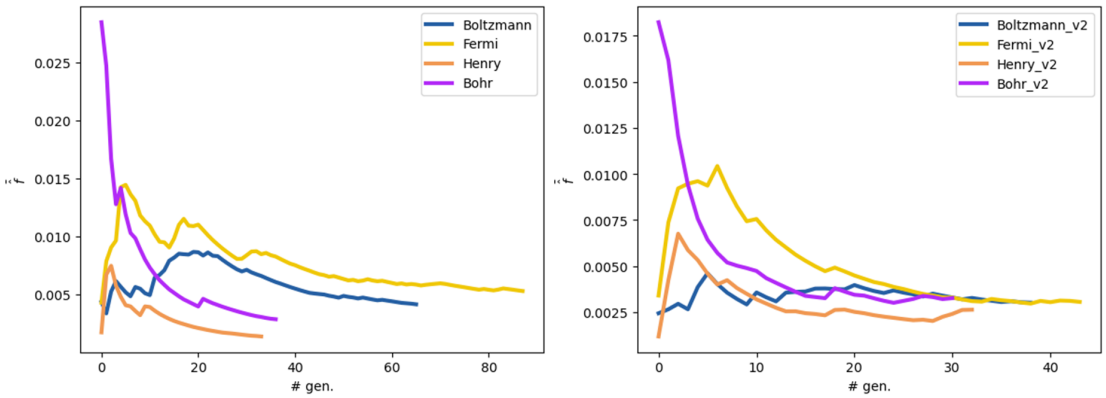

Figure 4.7: Convergence history of the average FF normalized with respect to the maximum joint FF, for the cases with 50 individuals per generation (left) and 100 individuals per generation (right)

In Figure 4.8 the distribution of the total number of individuals among the group boundaries is shown. The groups boundaries are numbered from the most energetic group, to the lowest ones. Again, the distribution among the boundaries seems slightly more uniform once the amount of individuals per generation increases, still preserving some consistent differences between the tribes. Instead, a shared feature is the low frequency with which high-energy boundaries are chosen, more specifically the ones between 3.679 and 0.821 MeV, which are associated with the energy range in which the power and flux peaks are met.

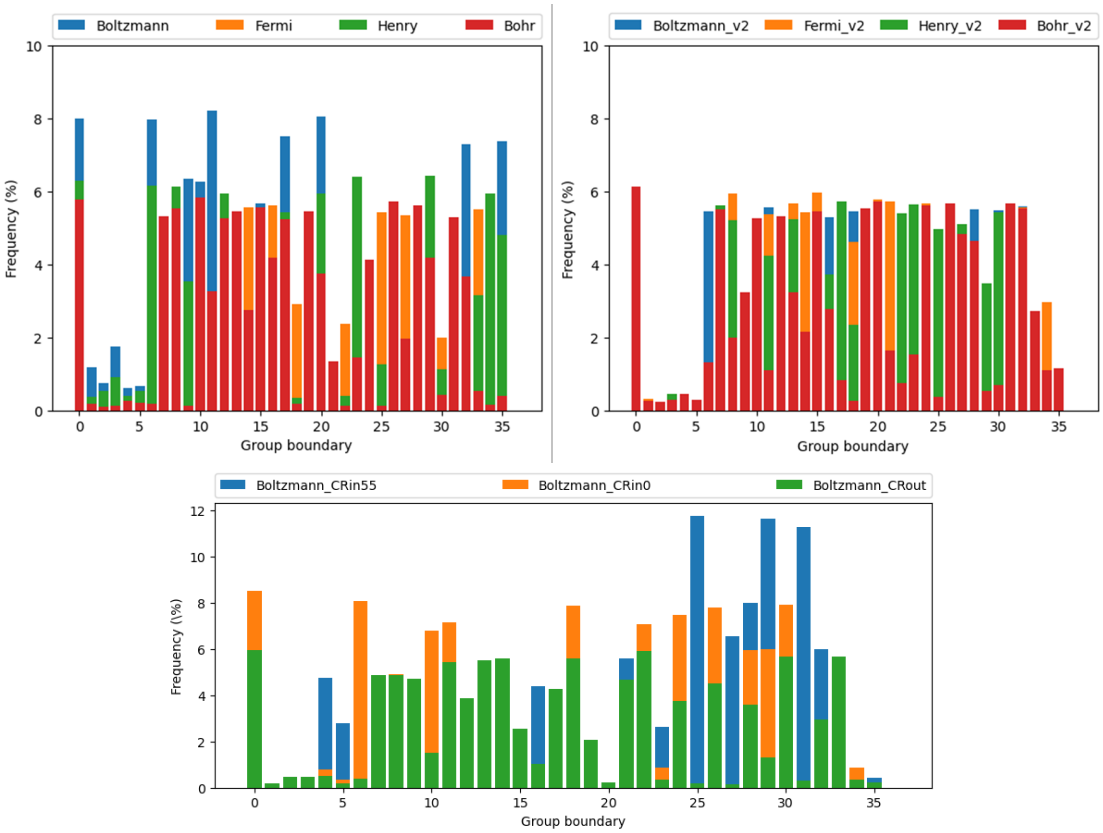

Figure 4.8: Distribution of individuals per groups boundaries through the whole evolution, for the multi-configuration cases (top) with 50 individuals per generation (left) and 100 individuals per generation (right), and the single configuration one (bottom).

Moreover, within 15 generations, the GA has already pushed the investigated solutions towards a high number of energy groups of the energy structure, and from that moment on, it seems to only explore the possible combinations of energy boundaries. The range on interest is in between 18 and 20 number of groups. This behavior stresses the importance of the chromosome structure definition, which allows to set the maximum number of groups. Indeed, the results suggest that the GA might have driven the solutions toward even higher number of energy groups, if such constraint had not been imposed, thus potentially leading to the violation of the hypothesis at the basis of the diffusion theory (if even finer starting energy grid would have been proposed).

Figure 4.10 represents the group boundaries making up the best individuals for

both the sets of simulations. It is possible to notice that the number of groups generally increases from roughly 15 groups up to almost 20. Simulations with a limited number of individuals per generation are characterized by energy boundaries confined within an energy range in between 10^{-3} and 20 MeV, where steeper power gradients appear. On the other hand, several energy boundaries belonging to the thermal and epithermal regions are then added when the number of individuals per generation is doubled. An encouraging feature of the results can be observed on best individuals evaluated by different seeds belonging to the same set of simulations, as they do not substantially differ one from the other, except for few energy boundaries.

Furthermore, it can be noticed that a certain relationship between the single-configuration and the multi-configuration optimization results holds. Indeed, high energy boundaries are poorly explored during the evolution for roughly the same energy interval, and they are not likely to appear in the best-performing individuals' coarse structure. On the other hand, many other energy boundaries are shared among the simulations.

With respect to the parameters that most influenced the simulations in producing the results previously discussed, their impact has been analyzed on a configuration-by-configuration basis, observing the evolution of the single fitness function per core configuration. The reason is that computing their product would have produced a range of values so wide that the key aspects related to the simulations' driving factors might have been obscured. In core configurations *CRout* and *CRin0*, the behavior of the fitness functions does not seem to substantially vary across the cases, suggesting that the predominant FFs influencing the selection of the number of energy groups are the ones associated with the k_{eff} and to β. In the configuration with the CRs fully inserted, the FFs behaviors mirror the ones already observed in the previous sections, being characterized by larger errors for a number of energy groups higher that 10.

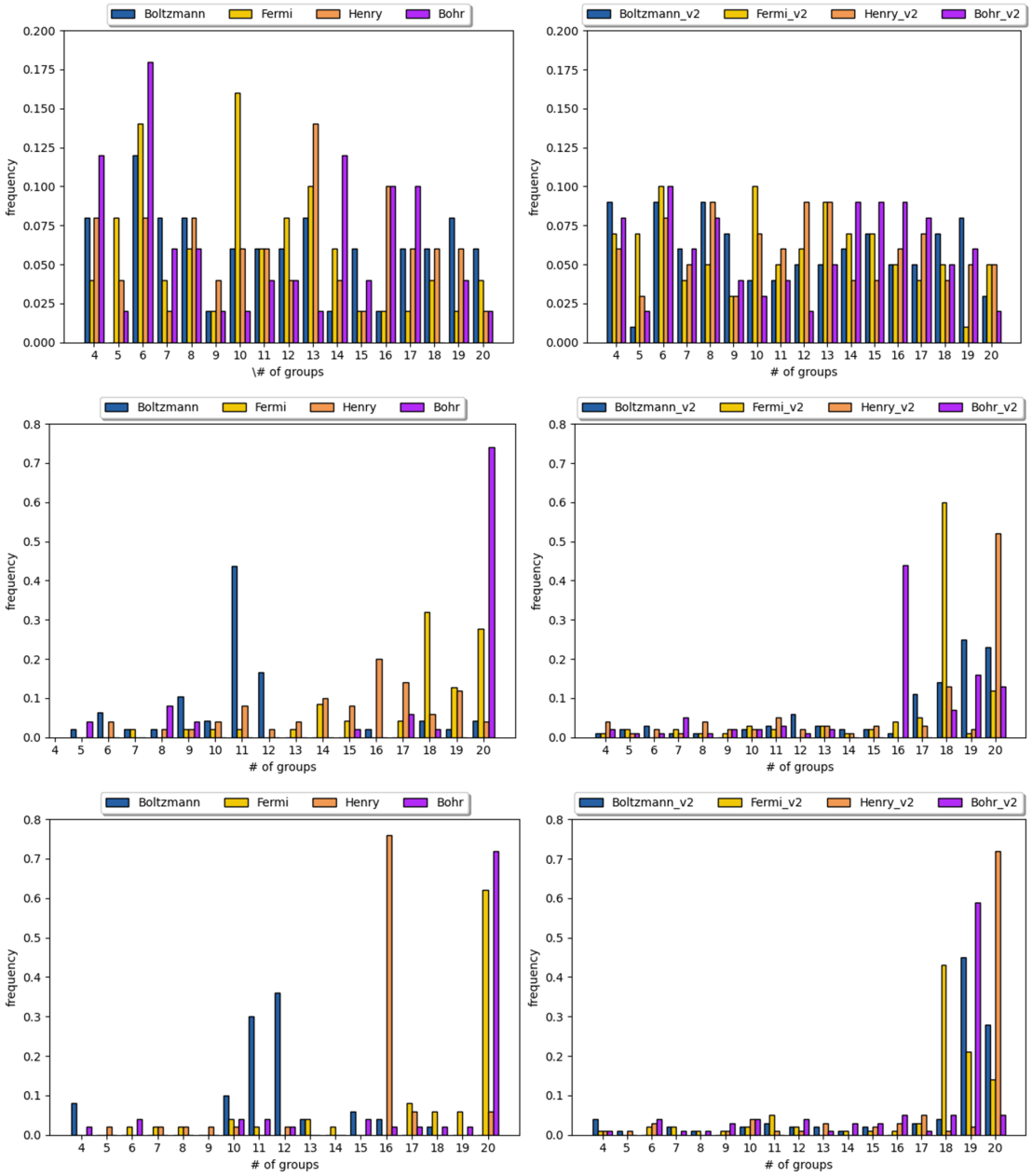

Figure 4.9: Distribution of individuals per number of groups at 0^{th} (top), 15^{th} (middle) and 30^{th} generation (bottom), for the cases with 50 individuals per generation (left) and 100 individuals per generation (right).

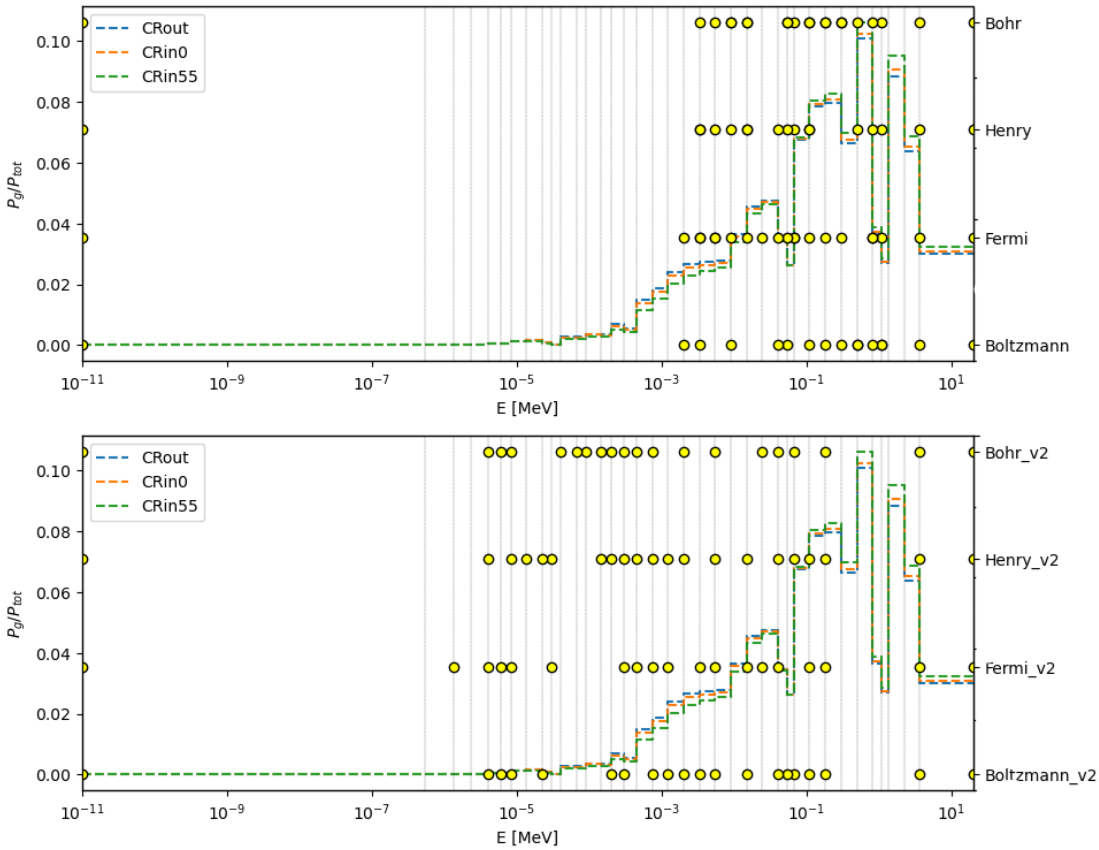

Figure 4.10: Best individuals of single-configuration cases against the power produced as a function of incident neutron energy. The dots represent the best individuals energy boundaries for different seed. The plots are referred to the case with 50 (top) and 100 (bottom) individuals per generation.

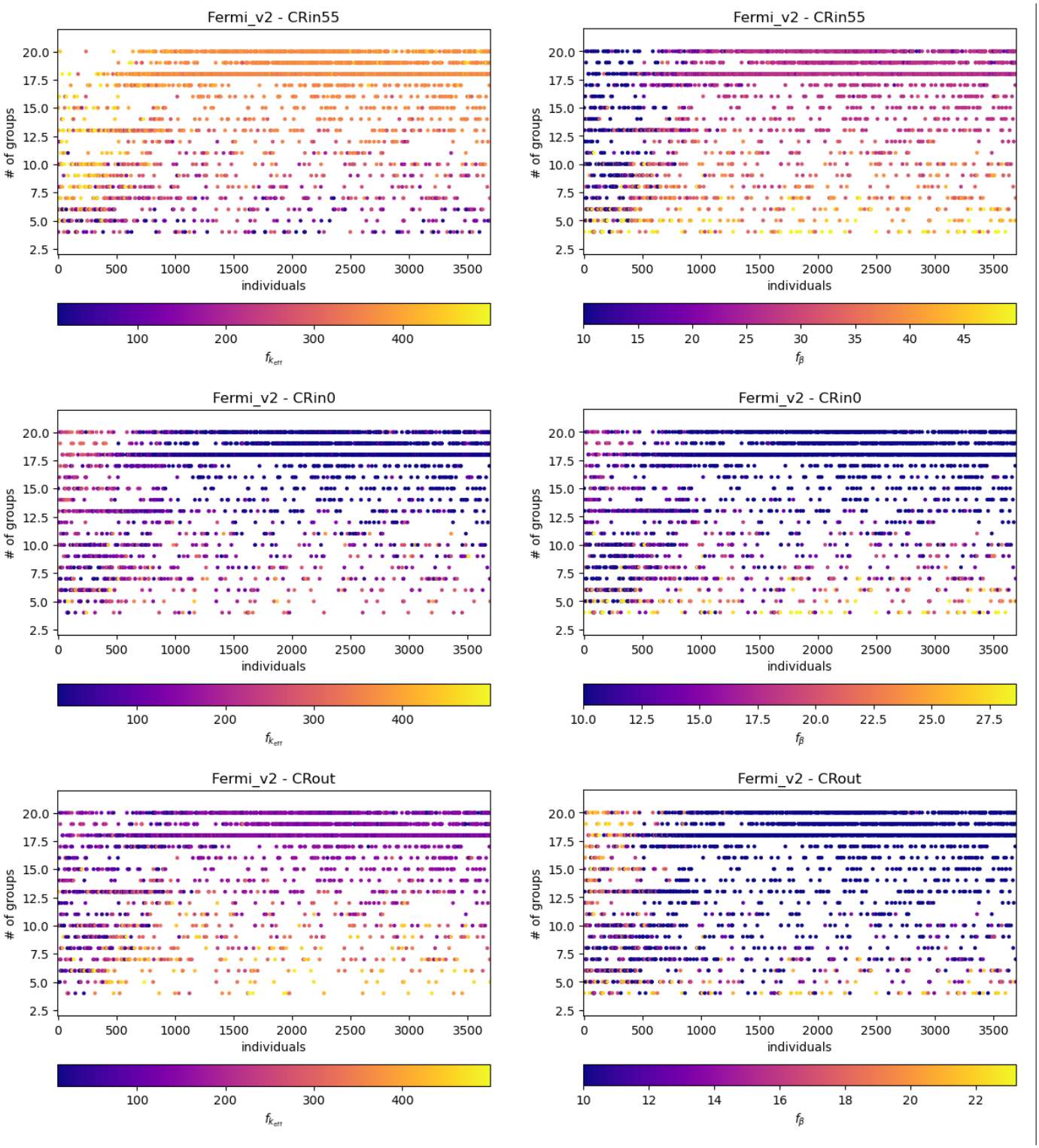

Figure 4.11: Fitness functions associated with k_{eff} (left) and β (right) for CRin55 (top), CRin0 (middle) and CRout (bottom) coming from the multi-configuration optimization.

Chapter 5

Conclusions and future perspective

Diffusion codes, like the FRENETIC, allow to strongly reduce the computational time required by full-core simulations, yet preserving an adequate solution accuracy. The identification of a proper energy group structure is fundamental to properly collapse the group constants to be fed to the diffusion codes. Generally, this is a crucial step as it may strongly affect the accuracy and efficiency of the multigroup calculations. Genetic Algorithms have revealed themselves to be powerful tools in solving this type of high-dimensional, non-linear optimization problems. Inspired by the working principle of Darwinian selection and evolution, the GA has been already explored in previous works, in the attempt of finding a proper energy structure to be applied to a specific configuration of the Advanced Lead Fast Reactor European Demonstrator (ALFRED), LEADER project. Based on the observed encouraging results, it has been interesting to evaluate and explore the performances and the possibilities associated with the use of such techniques, applying the algorithm to the new ALFRED benchmark, proposed by the Nuclear Energy Agency (NEA). To perform this study, the use of the multigroup diffusion module of the Fast REactor NEutronics/Thermal-hydrauliCs (FRENETIC) multiphysics code has been adopted, along with the Serpent2 Monte Carlo neutron transport code.

With respect to previous works [8], the specific aim of this thesis was trying to

identify an energy group structure to be shared by three different core configurations of the reactor, which are simultaneously optimized: one with the CRs fully withdrawn, one with CRspartially inserted, one with CRs fully inserted. Hence, three different 3D ALFRED Serpent2 models were build, and the starting energy group libraries were generated, based on a fine energy structure composed by 37 groups, whose boundaries were extracted by the XMAS-172 microgrid implemented in Serpent. The transport code was exploited to retrieve some relevant reference quantities. Then, the FRENETIC neutronic model was defined for each core configuration, and some preliminary simulations were performed to test the starting fine energy grid.

The Genetic Algorithm aimed at identifying the nearly-optimal solutions, i.e. coarser energy grids, by using a proper set of objective functions (*fitness functions, FF*), which allow to perform a proper ranking of the solutions identified through the optimization process. With respect to previous works in literature, FFs associated to kinetic parameters have been implemented in the code (β and Λ). Each core-configuration has been tested individually, as a frame of reference.

Results showed that the solution space becomes partially limited when the GA is required to find a solution shared across the three different core-configuration under investigation. As a consequence, the obtained solutions, although based on different initial seed, tend to exhibit a minimal variation one from the other, with the exception of few energy boundaries. While this aspect can be seen as encouraging (the convergence value is generally shared by the seed-based simulations), these solutions are characterized by energy group structure consisting of 19 groups. In the context of exploiting these solutions in transient or multiphysics simulations, this aspect may lead to cumbersome computational costs. To address this issue, it would be interesting to further modify the chromosomal parameter and analyzing the resulting solutions under the constraint of a lower maximum number of energy groups (ideally no greater than 10). In the perspective of testing the GA in its attempt of optimizing the energy structure of a multiphysics case, the starting set of energy group libraries were also generated (Tab. 2.3) with the intent of accounting for the feedback effect over the macroscopic cross sections. As a potential future development of this work, the capabilities of the genetic algorithm could be explored to optimize the axial discretization of the reactor core geometry,

in order to try to reduce the error introduced by material homogenization during the definition of the neutronic model a *priori.*

Bibliography

[1] R. Bonifetto, S. Dulla, P. Ravetto, L. Savoldi Richard, and R. Zanino. «A full-core coupled neutronic/thermal-hydraulic code for the modeling of lead-cooled nuclear fast reactors». In: *Nuclear Engineering and Design* 261 (2013), pp. 85–94. ISSN: 0029-5493. DOI: https://doi.org/10.1016/j.nucengdes.2013.03.030. URL: https://www.sciencedirect.com/science/article/pii/S0029549313001726 (cit. on p. 1).

[2] Jaakko Leppänen, Maria Pusa, and Emil Fridman. «Overview of methodology for spatial homogenization in the Serpent 2 Monte Carlo code». In: *Annals of Nuclear Energy* 96 (2016), pp. 126–136. ISSN: 0306-4549. DOI: https://doi.org/10.1016/j.anucene.2016.06.007. URL: https://www.sciencedirect.com/science/article/pii/S0306454916303899 (cit. on p. 2).

[3] George I. Bell and Samuel Glasstone. *Nuclear reactor theory / George I. Bell, Samuel Glasstone*. eng. New York: Van Nostrand, 1970 (cit. on pp. 2, 12).

[4] Ronald Allen Knief. *Nuclear Engineering - Theory and Technology of Commercial Nuclear Power (2nd Edition)*. eng. American Nuclear Society (ANS), 2014 (cit. on p. 13).

[5] G.Grasso. «EGPRS Lead-cooled Fast Reactor (LFR) Benchmark». In: (2023) (cit. on pp. 17, 26).

[6] G. F. Nallo, N. Abrate, S. Dulla, P. Ravetto, and D. Valerio. «Neutronic benchmark of the FRENETIC code for the multiphysics analysis of lead fast reactors». eng. In: (2020) (cit. on pp. 32, 33, 35).

[7] Dominic Caron, Roberto Bonifetto, Sandra Dulla, Piero Ravetto, Laura Savoldi, Domenico Valerio, and Roberto Zanino. «Full-core coupled neutronic/thermal-hydraulic modelling of the EBR-II SHRT-45R transient». eng. In: (2018) (cit. on p. 33).

[8] Nicolo Abrate and Alex Aimetta. *A genetic-driven optimisation of the energy grid structure for nodal full-core calculations in LFR (dataset)*. eng. 2024 (cit. on pp. 44, 46–48, 53, 69).

[9] A. Eiben and C. Schippers. «On Evolutionary Exploration and Exploitation». In: *Fundam. Inform.* 35 (Aug. 1998), pp. 35–50. DOI: 10.3233/FI-1998-35123403 (cit. on p. 44).

[10] Mattia Massone, Fabrizio Gabrielli, and Andrei Rineiski. «SIMMER extension for multigroup energy structure search using genetic algorithm with different fitness functions». kor. In: *Nuclear engineering and technology* 49.6 (2017), pp. 1250–1258. ISSN: 1738-5733 (cit. on p. 47).